Detection and Removal of Hyper-synchronous Artifacts in Massively Parallel Spike Recordings

Jonas Oberste-Frielinghaus[1,2,5*], Aitor Morales-Gregorio[1,5], Simon Essink[1,2], Alexander Kleinjohann[1,2], Sonja Grün[1,3,4], Junji Ito[1]

March 26, 2024

[1]Institute for Advanced Simulation (IAS-6), Jülich Research Centre, Jülich, Germany
[2]RWTH Aachen University, Aachen, Germany
[3]JARA-Institute Brain Structure-Function Relationships (INM-10), Jülich Research Centre, Jülich, Germany
[4]Theoretical Systems Neurobiology, RWTH Aachen University, Aachen, Germany
[5]These authors contributed equally
[*]Correspondence: j.oberste-frielinghaus@fz-juelich.de

Abstract

Current electrophysiology experiments often involve massively parallel recordings of neuronal activity using multi-electrode arrays. While researchers have been aware of artifacts arising from electric cross-talk between channels in setups for such recordings, systematic and quantitative assessment of the effects of those artifacts on the data quality has never been reported. Here we present, based on examination of electrophysiology recordings from multiple laboratories, that multi-electrode recordings of spiking activity commonly contain extremely precise (at the data sampling resolution) spike coincidences far above the chance level. We derive, through modeling of the electric cross-talk, a systematic relation between the amount of such hyper-synchronous events (HSEs) in channel pairs and the correlation between the raw signals of those channels in the multi-unit activity frequency range (250-7500 Hz). Based on that relation, we propose a method to identify and exclude specific channels to remove artifactual HSEs from the data. We further demonstrate that the artifactual HSEs can severely affect various types of analyses on spiking train data. Taken together, our results warn researchers to pay considerable attention to the presence of HSEs in spike train data and to make efforts to remove the artifacts from the data to avoid false results.

Introduction

Modern electrophysiological experiments often use multi-electrodes, such as Utah arrays (Blackrock Microsystems, Salt Lake City, UT, USA) (Hatsopoulos et al., 1998; de Haan et al., 2018; Chen et al., 2022) and Neuropixels probes (Cambridge NeuroTech, Cambridge UK) (Jun et al., 2017), to record neuronal activity at multiple sites simultaneously. These recordings are known to be very sensitive to various sources of noise (Rey et al., 2015; Harris et al., 2016), which need to be mitigated to enable reliable and robust data analysis. Signal artifacts in neural recordings occur from both internal (heartbeats, eye movements, chewing etc.) and external (electric grid interference, loud noises etc.) sources (Fabietti et al., 2020). These sources are of non-neural origin, and can often be distinguished from neural activity owing to their particular frequencies and distinct waveforms. Common removal methods are based on independent component analysis (Bell & Sejnowski, 1995; Rong & Contreras-Vidal, 2006; Delorme et al., 2007), canonical correlation analysis (Hotelling, 1936; Wim De Clercq et al., 2006), wavelet methods, or certain combinations thereof. These are mostly applied to electroencephalogram (EEG) (Wim De Clercq et al., 2006; Delorme et al., 2007; Shackman et al., 2009; Barban et al., 2021; Mumtaz et al.,

2021) and magnetoencephalogram (Rong & Contreras-Vidal, 2006) data, and to a lesser extent to extracellular electrophysiology (Ludwig et al., 2009; Islam et al., 2014; Fabietti et al., 2020).

Besides these common noise sources, capacitive coupling between shanks or cables can cause cross-talk between different channels (Nelson et al., 2017), leading to a mixing of neural signals that can persist even after spike sorting (Torre et al., 2016). Cross-talk is a well-known problem in EEG (Nagaoka et al., 1992) and electromyogram (Koh & Grabiner (1993); Kilner et al. (2002); Farina et al. (2004)) data recording systems. Yet, to the best of our knowledge, only a few studies have focused on cross-talk in electrophysiology systems (Musial et al., 2002; Nelson et al., 2017; Pérez-Prieto & Delgado-Restituto, 2021). One approach to avoid cross-talk in these systems is through hardware implementations, like improving the isolation and design of the circuits (Blot & Barbour, 2014; Nelson et al., 2017; Pérez-Prieto & Delgado-Restituto, 2021; Perez-Prieto et al., 2021). However, most neuroscientists do not design their own custom hardware and thus the effects of cross-talk have to be mitigated with post-hoc methods.

One artifact linked to cross-talk is extremely precise (at the data sampling resolution, e.g. $\frac{1}{30}$ ms) spike synchrony (Yu et al., 2009; Torre et al., 2016; Dehnen et al., 2021; Chen et al., 2022). Spiking activity is known to be coordinated on the timescales of a few milliseconds (König et al., 1995; Riehle et al., 1997; Butts et al., 2007; Grün, 2009), but no observation of sub-millisecond coordination has been reported, nor are there any known mechanisms that enable sub-millisecond synchronization. Furthermore, the separation between electrodes in those studies was $\geq 400\,\mu$m, well beyond the spatial reach of extracellular electrodes (Henze et al., 2000), denying the possibility that the apparent sub-millisecond synchronization is merely an identical spike recorded by multiple electrodes. Therefore, these hyper-synchronous events were considered artifacts, which we name here *synchrofacts* (short for synchronous artifacts).

Some studies remove suspicious spikes from further analysis either during the spike sorting process (Musial et al., 2002; Dann et al., 2016) or post-hoc (Torre et al., 2016; Dehnen et al., 2021). Other studies remove entire channels or neurons instead (Churchland et al., 2006; Yu et al., 2009; Snyder et al., 2021; Chen et al., 2022; Semedo et al., 2022; Morales-Gregorio et al., 2023). However, most removal methods are relatively complex, computationally expensive, and might require manual verification of the results.

To overcome the limitations of the above mentioned methods, we here show that cross-talking channels can be detected from both the raw signal cross-correlation and the degree of spike coincidence. Our detection method is tested on two extracellular electrophysiology data sets from two different experimental laboratories (de Haan et al., 2018; Chen et al., 2022). A theoretical model confirms that the experimental observations are consistent with what is expected from cross-talk between recording channels. Furthermore, we propose and evaluate several methods to remove synchrofacts based on our metrics. Finally, we demonstrate that the presence of synchrofacts can radically affect analysis results: on a) estimation of neuronal tuning curves and on b) Unitary Event analysis (Grün et al., 1999, 2002a,b; Grün, 2009) for detection of excess spike synchrony. The application examples highlight the need for the detection and removal of synchrofacts. All in all, our methods construe a novel and simple approach to synchrofact removal that can be applied to any multi-electrode recording system to ensure cleaner and more reliable data.

Results

Synchronous spike events are ubiquitous in multi-electrode systems

To demonstrate how synchrofacts appear in massively parallel spike train data, we inspect two data sets from two different laboratories and monkeys (Figure 1a). In the dot-display of the simultaneously recorded spike trains (Figure 1b, top), we notice events where many neurons exhibit spikes simultaneously (highlighted in gray). To examine the temporal scale of these events, we compute the population spike time histograms with different bin sizes (Figure 1b, bottom). At the resolutions of 1 ms and $\frac{1}{30}$ ms, we find some bins with outstandingly high spike

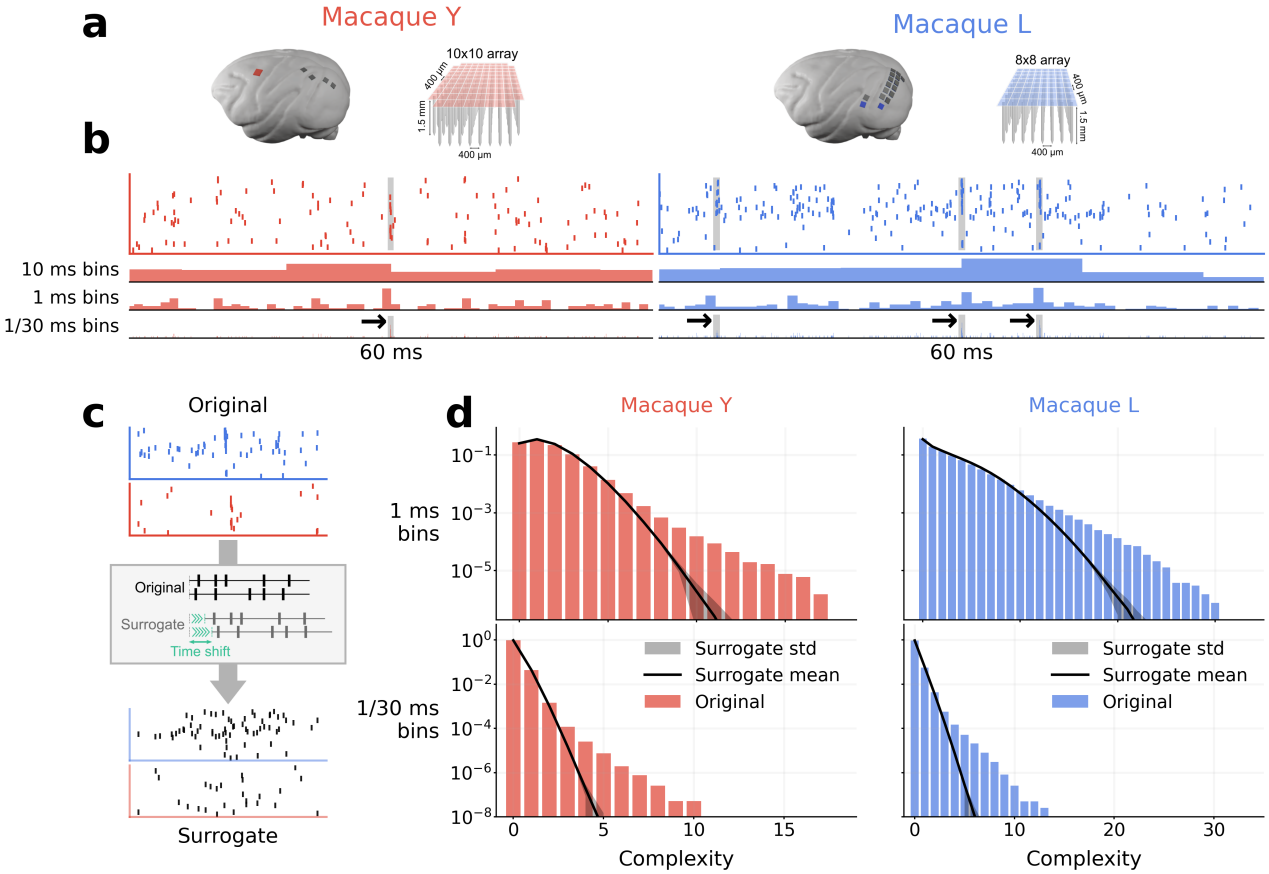

Figure 1: Observation of hyper-synchronous event (HSEs). (a) Electrode arrays and implantation sites for the two macaques, macaque Y: 6x6 electrode arrays in V1, V2, DP, 7A and 10x10 in M1/PMd (we focus here only on the 10x10 array); macaque L: 14 8x8 arrays in V1 and two in V4 (focus here on an array pair with one in V1 and one in V4). The arrays focused on are colored. (b) Dot display (top) and population histograms with different bin sizes (bottom) for a 60 ms long data slice. HSEs are highlighted with gray. (c) Illustration of the surrogate generation method. Original spike trains are shifted against each other by a random amount of time. (d) Complexity distribution of the original data (colored bars), and the mean and standard deviation (line and shade, respectively) for the complexity distribution of the respective surrogates. Top: 1 ms bin size; bottom: $\frac{1}{30}$ ms bin size.

counts, not visible at the resolution of 10 ms. Whereas neurons can coordinate their activity with millisecond precision (König et al., 1995; Riehle et al., 1997; Butts et al., 2007), to the best of our knowledge, no neural mechanism has been reported to produce synchronization within $\frac{1}{30}$ ms. We term these extremely precise spike coincidences as hyper-synchronous events (HSEs).

We further quantify the HSEs by their complexity (i.e., number of involved neurons) (Grün et al., 2008) and compare the obtained complexities to those expected by chance using a surrogate method (Stella et al., 2022)(Figure 1c; see STAR Methods for details). Figure 1d shows the distributions of complexity values from the original and the surrogate data, for two different bin sizes (1 ms and $\frac{1}{30}$ ms). For both bin sizes, the original data contains much more events with high complexities than the surrogate data Thus, HSEs occur by chance much less than what we observe in the experimental data. Considering that the coordination of spike times on the timescale of $\frac{1}{30}$ ms is very unlikely, we conclude that many of the HSEs in the experimental data are artifacts, which we name synchrofacts.

We find synchrofacts in two separate data sets originating from two different laboratories, recorded in two different cortical areas of different monkeys. Therefore we suspect that synchrofacts are common across recordings of the same type. While both data sets were recorded with Blackrock recording systems, it has been reported

that synchrofacts also occur in other recording systems, e.g. in Neuropixel recordings (Jain et al., 2022). Taken together, our observations and previous reports highlight the ubiquity of synchrofacts.

One might think that the data can be cleaned by simply removing all HSEs. However, that is not an appropriate solution to get rid of synchrofacts, since this also removes many genuine neuronal spikes and neural synchrony. One can demonstrate this by removing all spikes in the bins with complexity of two or larger at $\frac{1}{30}$ ms resolution, and then calculating the complexity distribution, to compare it to the surrogate complexity distribution. The surrogate distribution obtained in this way contains complexities of two or higher that occur by chance. However, the original distribution totally lacks complexities higher than 2, and hence it differs vastly from the surrogate distribution (see Supplementary Figure S1). Thus, removing all HSEs alters the statistic properties of the spike trains significantly, which can lead to false results regarding fine temporal correlations.

To summarize, HSEs in massively parallel spike trains commonly contain synchrofacts, which are artifactual spike coincidence events on a timescale of the data sampling frequency. They can only be spotted when analyzing the data on very fine timescales and show themselves as an excess of HSEs. Since HSEs contain not only synchrofacts but also genuine neuronal synchrony (as well as chance coincidences), removing all HSEs for cleaning the data is not a proper approach. Hence, we aim at selectively removing synchrofacts from the data, and to this end, we need to discriminate synchrofacts from chance coincidences of real spikes.

Synchronous spike events with nearly identical raw signals are not of neural origin

Following the observations in the previous section, we now take a deeper look into the HSEs for features discriminating synchrofacts from chance spike coincidences. Whereas an HSE with a very high complexity is likely to be a synchrofact, we cannot rule out the possibility that it is a real spike synchrony. In fact, there is no way of discriminating between them on the description level of spikes. Thus, seeking for additional information to spot synchrofacts, we inspect the raw signals from which the spike events are extracted.

The spike extraction was done by thresholding the band-pass filtered raw signals in the frequency range of 250 Hz − 7500 Hz (see Signal processing and threshold crossings in STAR Methods for details). For simplicity, we henceforth refer to the band-pass filtered raw signal merely as raw signal, unless noted otherwise. Figure 2a shows the raw signals of multiple channels around the timing of one HSE. We observe highly similar spike-like waveforms in multiple channels simultaneously, but with different amplitudes. Furthermore, the ongoing signal fluctuations before and after the HSE appear to be correlated across these channels. The electrodes of these channels are not necessarily in close spatial proximity, as shown in Figure 2b. We measure the distances between the electrodes of channels participating in each and every HSEs with high complexities, and observe that the high complexity HSEs often involve electrodes that are far apart, up to several millimeters (Figure 2c). In particular, in the case of macaque L, HSEs appear even across the two arrays located on opposite banks of the lunate sulcus.

To summarize, we have observed i) sub-millisecond synchronization of spikes across channels, ii) the nearly identical waveforms of those spikes, iii) the visible correlation between raw signals, and iv) the large distance between the participating electrodes. Taken together, these observations strongly suggest that many of these events are artifacts due to electric cross-talk between channels, rather than multiple electrodes recording the same neuron or some novel form of fast neuronal synchronization.

Cross-correlation and hyper-synchronous events can detect synchrofacts

An electric cross-talk between a channel pair is expected to increase the Pearson correlation coefficient between the raw signals of these channels. Figure 3a shows the raw signal correlation coefficient $c_{i,j}$ between channels i and j (see Cross-correlation of high-pass filtered raw signals in STAR Methods for details) for all channel pairs in the two data sets in a matrix form (only for $i \neq j$), and Figure 3b the distribution of the $c_{i,j}$ values in the matrix. The coefficients are mostly larger than zero, i.e., the raw signals are generally positively correlated. The coefficient values vary strongly across channel pairs, with some pairs showing quite strong correlation, in both

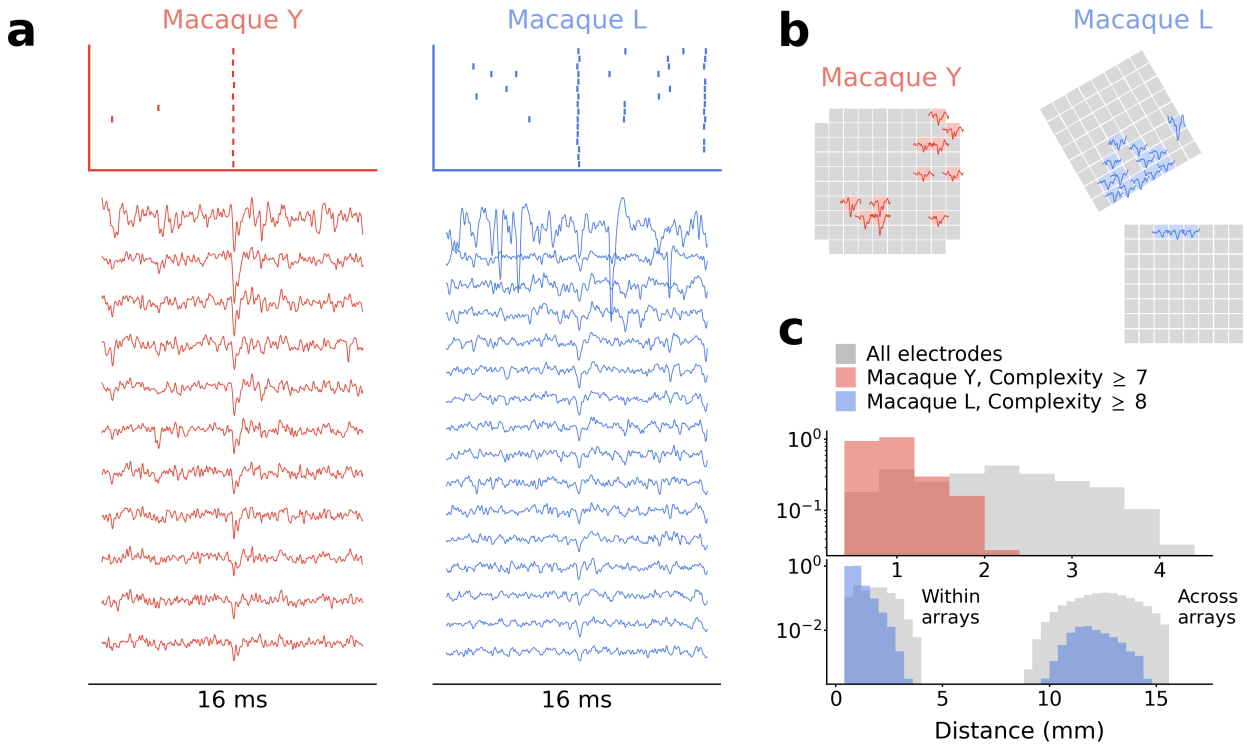

Figure 2: HSEs in relation to the raw signals, for macaque Y (red) and L (blue). (a) Dot display (top) centered around a single HSE and the corresponding band-pass filtered (250 Hz - 7500 Hz) raw signals of the channels participating in the HSE. Spike-like excursions are aligned on the HSE. (b) Positions of the electrodes on the respective array for the raw signal channels participating in the HSE in (a). The trace of the spike-like excursion in each channel is shown at the corresponding position. (c) Distances between the electrodes involved in all HSEs with high complexity, selected based on the surrogate analysis from Figure 1. For reference, the distance distribution between all possible electrode pairs is shown in gray.

recording setups from different laboratories.

There may be multiple possible origins for such strong correlations, ranging from damages on the electrodes to electric shortcuts between channels due to various reasons, e.g., crossing of the implanted cables below the skull, dirt in the headstage connector, interference between the cables connected to the amplifier, etc. (Yu et al., 2009). As shown in Figure 2b and c, the artifacts are not limited to spatially proximal channels but extend over the whole array or even across arrays, indicating that a deficit in a local group of channels cannot be the primary reason for these correlations. Another possibility is a local deficit on the headstage connector, but this is also denied by examining the spatial extent of correlated channels mapped on the connector (see Macaque L data in Supplementary Figure S2). Thus, no single reason can explain the observed correlations, but rather there would be multiple causes residing on different stages of the setup. Eliminating all possible causes from the setup is practically not feasible, and hence we cannot avoid having such correlations in the data.

Excluding the channels with strong correlations from the analysis would be easy, if their correlation coefficients were distinctly different from the other channels. However, the distribution of the correlation coefficient values typically shows a smooth decay towards high values (Figure 3b), indicating no clear critical correlation coefficient value above which the respective channel pairs are considered to be problematic.

To find an appropriate value for such a critical correlation, we examine the relation between the raw signal correlation $c_{i,j}$ and the spike coincidences in the respective raw signals. For channel pairs with a large $c_{i,j}$ value, their raw signals must be similar to each other. Hence, if one channel of such a pair had spike-like waveforms, the other channel should also have those at the same time. This leads to the expectation that a channel pair with a larger $c_{i,j}$ should show more synchrofacts. To confirm this, we first count, for each channel pair, the number of HSEs containing spikes from that pair. We then define the HSE index $I_{i,j}$ of channel i and j as the ratio of the obtained HSE count to the spike counts of these two channels (see Measure of spike synchrony in STAR Methods for the formula). Figure 3c shows the $I_{i,j}$ values obtained from the two data sets in a matrix form (only for $i \neq j$), and Figure 3d the distribution of those values in the matrix. We find $I_{i,j}$ values ranging from zero to 0.5, while the value expected from an independent pair of spike trains is of order of magnitude 10^{-3} (see Supplementary Figure S3).

We then plot $I_{i,j}$ against the correlation coefficients c_{ij} to look for a systematic relation between them (Figure 3e). We find that a majority of channel pairs have HSE index values close to zero, meaning that hardly any spikes are shared by these pairs. Especially the channel pairs with low correlation coefficients $c_{i,j}$ such as < 0.4 have very low HSE index values. As the correlation $c_{i,j}$ gets larger than 0.4, the HSE index value rapidly increases, indicating a critical correlation beyond which spikes becomes very likely to be detected in both channels. Note that an HSE index larger than zero does not immediately indicate synchrofacts. As shown in (Figure 1d), a certain amount of HSEs can be explained by chance. However, as we mentioned before, the HSE index expected from independent spike trains is very small, on the order of 10^{-3}. Hence, an HSE index excessively greater than this strongly indicates presence of synchrofacts.

Cross-talk model explains the emergence of synchrofacts

To understand the origin of the relation between the raw signal correlation and the HSE index, here we present a simple model of cross-talk between channels (see Cross-talk model in STAR Methods for details). This model enables us to derive an analytic expression of the relation, which is in agreement with our experimental observations (Figure 3e).

Our model assumes two Gaussian white noise (mean 0, variance σ^2) time series x_1 and x_2 as the cross-talk-free "ground truth" signals. We model the cross-talk as a linear mixing of these two signals (Figure 4a), such that the measured signals s_1 and s_2 of channel 1 and 2, respectively, are:

$$\begin{aligned} s_1 &= x_1 + \alpha x_2 \\ s_2 &= x_2 + \alpha x_1, \end{aligned}$$

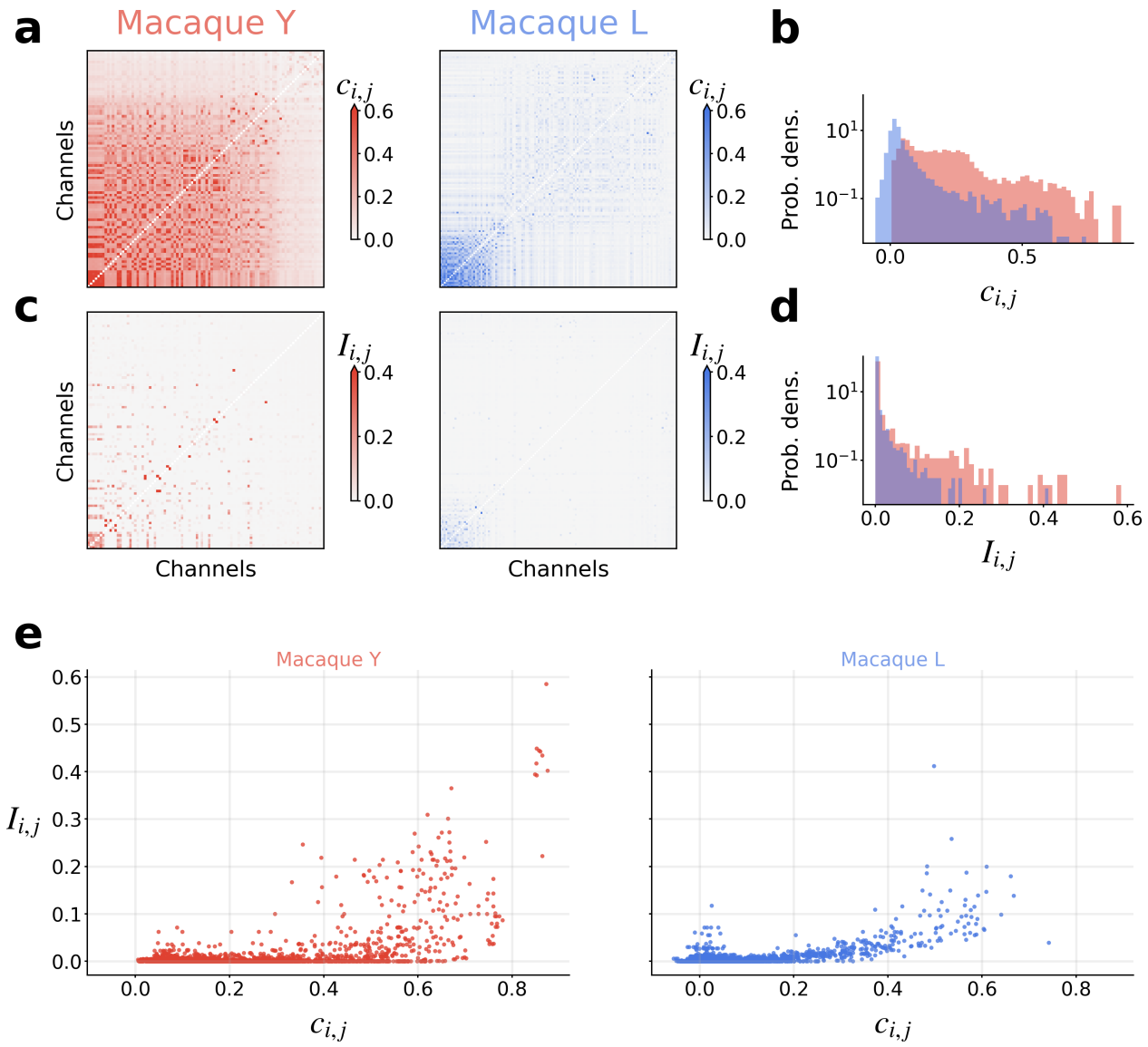

Figure 3: Relation of pairwise raw signal correlations to respective pairwise occurrences of HSEs. (a) Pairwise correlation coefficients $c_{i,j}$ of the raw signals. Data are shown in matrix form; the channels are sorted by largest maximum correlation. (b) Distribution of the $c_{i,j}$ values that appear in the matrix shown in (a). (c) HSE index $I_{i,j}$ for all channel pairs shown in a channel-by-channel matrix form. The channels are sorted in the same order as in (a). (d) Distribution of the $I_{i,j}$ values that appear in the matrix shown in (c). (e) Scatter plot of the raw signal correlation coefficient $c_{i,j}$ against HSE index $I_{i,j}$ of the corresponding channel pair. Each dot represents one channel pair.

where $0 \leq \alpha \leq 1$ is the strength of the cross-talk: s_1 and s_2 are identical with $\alpha = 1$, and independent with $\alpha = 0$. The Pearson correlation coefficient $c_{1,2}$ between s_1 and s_2 can be written in terms of α as (see Cross-talk model in STAR Methods for derivation):

$$c_{1,2} = \frac{2\alpha}{1+\alpha^2}. \tag{1}$$

Thus the correlation $c_{1,2}$ increases nonlinearly with the cross-talk strength α (see Figure 4b).

For the derivation of the HSE index, we need to introduce spikes to the signals. We model spikes by subtracting a value A_i, representing the spike amplitude, from the ground truth signal x_i at random time points ($i \in \{1,2\}$). We parameterize A_i as $A_i = \sigma r_i^{\mathrm{SN}}$, where r_i^{SN} is the signal-to-noise ratio of the spike waveform in x_i. Spikes are then extracted from the measured signals s_1 and s_2 by thresholding, as commonly done for experimental data. We set the threshold for s_i at $-m\sigma_{s_i}$, where $\sigma_{s_i} = \sqrt{1+\alpha^2}\sigma$ is the standard deviation of s_i and m is a multiplier (Quiroga et al., 2004). The expected numbers n_1 and n_2 of spikes detected in s_1 and s_2 are:

$$\begin{aligned} n_1 &= p_{1,1}\left(\alpha, r_1^{\mathrm{SN}}, m\right) N_1 + p_{1,2}\left(\alpha, r_2^{\mathrm{SN}}, m\right) N_2 \\ n_2 &= p_{2,1}\left(\alpha, r_1^{\mathrm{SN}}, m\right) N_1 + p_{2,2}\left(\alpha, r_2^{\mathrm{SN}}, m\right) N_2, \end{aligned}$$

where N_1 and N_2 are the number of spikes introduced in x_1 and x_2, and p_{ij} are the probabilities that a spike from x_i is detected in s_j, see Cross-talk model in STAR Methods for more details.

The spikes transferred across channels by the cross-talk are detected in both channels, so the sum of the numbers of such spikes, i.e., $n_{1,2} = p_{1,2}N_2 + p_{2,1}N_1$ represents the number of synchrofacts in this pair of channels. We can now calculate the HSE index as $I_{1,2} = n_{1,2}/\min(n_1, n_2)$ (see Cross-talk model in STAR Methods for detailed derivations).

Through the dependence of $p_{i,j}$ on the cross-talk strength α, the HSE index $I_{1,2}$ is dependent on α and thereby the correlation coefficient $c_{1,2}$ (Figure 4c). Interestingly, no synchrofacts are observed in the model for $\alpha < 0.2$ or $c_{1,2} < 0.4$, suggesting that some degree of cross-talk might be tolerable in recording systems. However, for higher α or $c_{1,2}$, the HSE index rapidly increases in the form of a sigmoid, depending on the signal-to-noise ratio r^{SN}.

So far we have grouped spikes in one channel into a single class, i.e., spikes that originate from different ground truth signals (and therefore from different neurons) were not discriminated. In analyses of real spike train data, however, researchers are often interested in examining properties of the spiking activity of a single individual neuron, i.e., single unit activity (SUA). SUA spikes are sorted out from a spike train in a single channel, based on the waveforms of individual spikes. The original spike train before the sorting potentially contains spikes from multiple different neurons, termed multi-unit activity (MUA). In our analyses so far, the HSE index has been computed based on the MUA spikes of a pair of channels. We can instead consider the HSE index between a pair of individual SUAs, in the same manner as for the MUAs.

Let us examine how the HSE index for SUA pairs differs from that for MUA pairs, for the case shown in Figure 4a. Here only one SUA (blue spikes) is detected in channel 1, while in channel 2 two SUAs (blue and orange spikes) could be detected, if the spike waveforms differed distinctly enough for successful spike sorting. Here we assume that these spikes are correctly sorted, and consider the HSE index between SUA11 and SUA21 shown in Figure 4a, and between SUA11 and SUA22 (note that the HSE index between SUA21 and SUA22 is zero, since there can be no HSEs between SUAs on the same channel.) For the SUA11-SUA21 pair, all their spikes originate from x_1, and hence all SUA21 spikes (i.e., the spikes transferred from x_1 to s_2) are found in SUA11 at the same spike times. Thus, the HSE index for this SUA pair is 1. Note that this is generally the case for any pair of SUAs that originate from a single ground truth signal and bleed into different channels due to the cross-talk. On the other hand, the HSE index for the SUA11-SUA22 pair should be as small as expected from chance coincidences, since these SUAs represent spikes of independent neurons in different ground truth signals. This is generally the case for any pair of SUAs that originate from different ground truth signals.

To summarize, the HSE index between SUAs can only take a value of either 1 or as a small number as expected

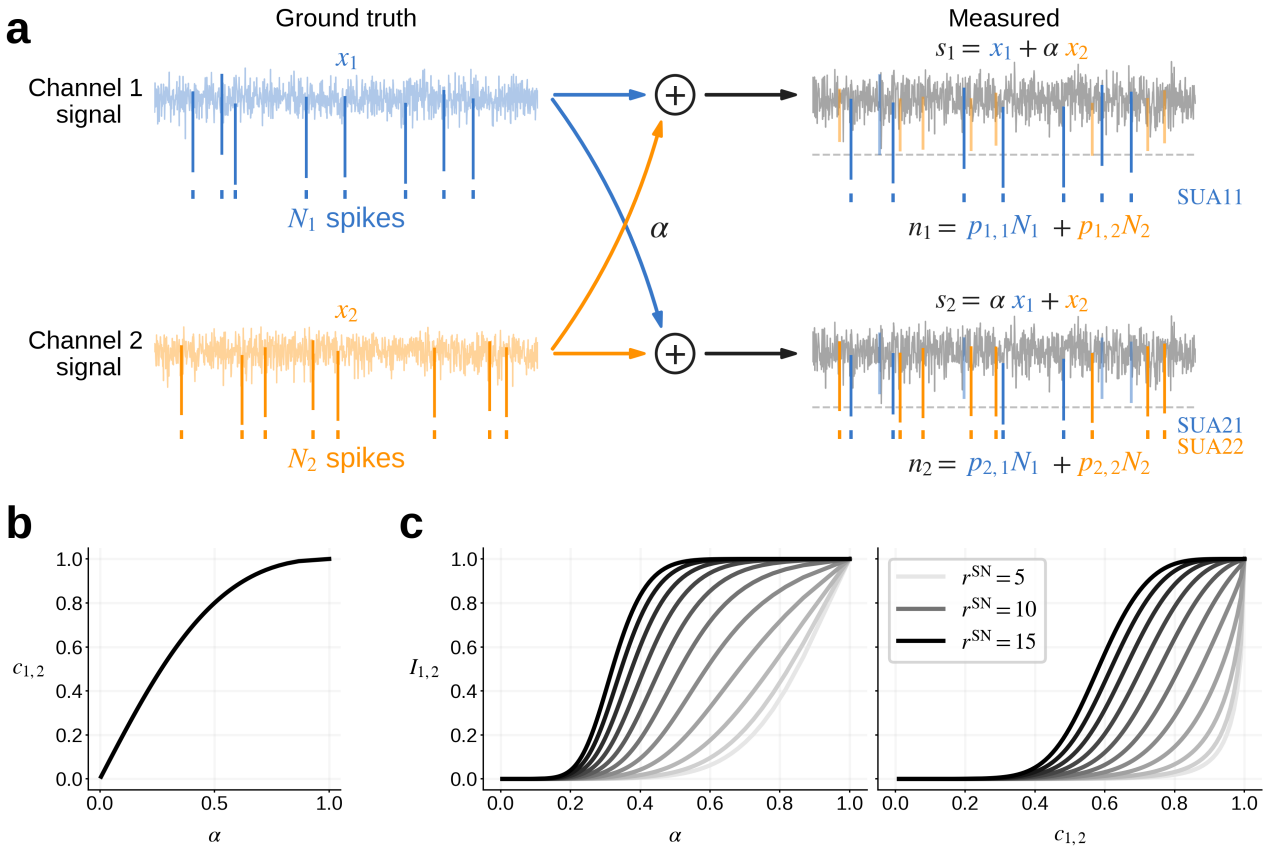

Figure 4: Cross-talk model of synchrofacts. (a) Illustration of the setup for derivation of the synchrofact index. Ground truth signals for channels 1 and 2 are mixed, representing the cross-talk, to yield the signals measured in a pair of channels. Spikes (vertical lines) are introduced to the ground truth signals, and they "bleed" into the measured signal of the other channel via the cross-talk. (b) The correlation $c_{1,2}$ between the channels plotted against the cross-talk strength α. (c) The HSE index $I_{1,2}$ of the channels plotted against the cross-talk strength α (left) and the correlation $c_{1,2}$ between the channels (right). Here the signal-to-noise ratios of spikes in x_1 and x_2 are set to be identical $r_1^{\mathrm{SN}} = r_2^{\mathrm{SN}} = r^{\mathrm{SN}}$, and varied between 5 and 15 in steps of 1, while keeping the threshold multiplier at $m = 5$. The curves for different values of r^{SN} are plotted in different shades of gray.

from chance coincidences. This conclusion applies to any pair of SUAs as long as spike trains are perfectly sorted into SUAs in all channels. Thus, any intermediate values of HSE index between these two can only happen when the index is computed for a MUA pair. If such HSE values were obtained between SUAs, that would indicate that the spike sorting is not perfect and some SUAs contain spikes bleeding from other channels due to the cross-talk.

Channel removal for synchrofact mitigation

We now consider how we utilize the knowledge from the model to remove synchrofacts from the data. Let us first consider the case with unsorted MUA spikes. In this case, the model indicates more synchrofacts in channel pairs with stronger raw signal correlation. Thus, one approach to remove synchrofacts in this case would be to discard the MUAs of channels strongly correlated with any other channel(s). For such screening of channels, we identify the highest correlation coefficient for each channel, denoted as C_i for channel i and defined as:

$$C_i = \max_{j \neq i}(c_{i,j}), \tag{2}$$

where $c_{i,j}$ denotes the correlation coefficient between the raw signals of channel i and j. We then choose a threshold value on C_i, such that all channels with C_i values above this threshold are excluded. Since the model shows that the HSE index grows rapidly as the correlation coefficient increases beyond 0.4 (see Cross-talk model explains the emergence of synchrofacts in Results), we set the threshold on C_i at 0.4.

To see how the channel-wise highest correlation coefficient C_i is related to occurrences of HSEs in channel i, we introduce yet another measure evaluating the participation of each channel in HSEs. We term this as the global HSE index I_i for channel i, defined as the ratio of the number of HSEs including channel i to the number of all spikes on channel i (see Measure of spike synchrony in STAR Methods for the formula). The HSE index $I_{i,j}$ that we have introduced before for a pair of channels i and j is henceforth referred to as pairwise HSE index. Figure 5a (left) shows the global HSE indices I_i plotted against their respective highest correlation coefficients C_i for all channels in macaque Y and L data sets. As expected from the model, the channels with high C_i values are indeed also the channels with high I_i values, while the channels with C_i below 0.4 show rather small I_i.

As proposed above, we now exclude all channels with C_i values higher than 0.4 to remove synchrofacts. For the present data sets this excludes a lot of channels from the analysis. For example, in the case of macaque Y, more than a half of the channels are excluded (Figure 5b). After discarding MUAs on those channels, the complexity distribution matches the expectation from chance coincidences (Figure 5c, middle), indicating that synchrofact HSEs are successfully removed (together with all the spikes on the excluded channels) while keeping chance HSEs on the remaining channels intact.

Among the channels excluded above, there are a considerable number of channels showing low I_i values comparable to those of the channels kept for analyses (Figure 5a, middle). According to the model, these would be the channels with spikes of such small amplitudes that they do not cause synchrofacts (because they do not cross the threshold even if they bleed into other channels), and not receiving spikes from other channels either. If this is the case, these channels should be kept in analyses, since they contain only the spikes recorded at their respective electrodes. This leads to an idea of channel screening by thresholding not on C_i, but on I_i. Therefore we devise a second method to exclude channels as follows: 1) set a threshold for C_i; 2) take the highest of the I_i values for all the channels with C_i below this threshold; 3) exclude all channels with an I_i higher than the value taken in (2). This excludes considerably less channels than the previous method (Figure 5b), but is similar in results with regard to the complexity distribution (Figure 5c). Thus, regardless of which method we choose, if we exclude the right channels, we can avoid most of the synchrofacts.

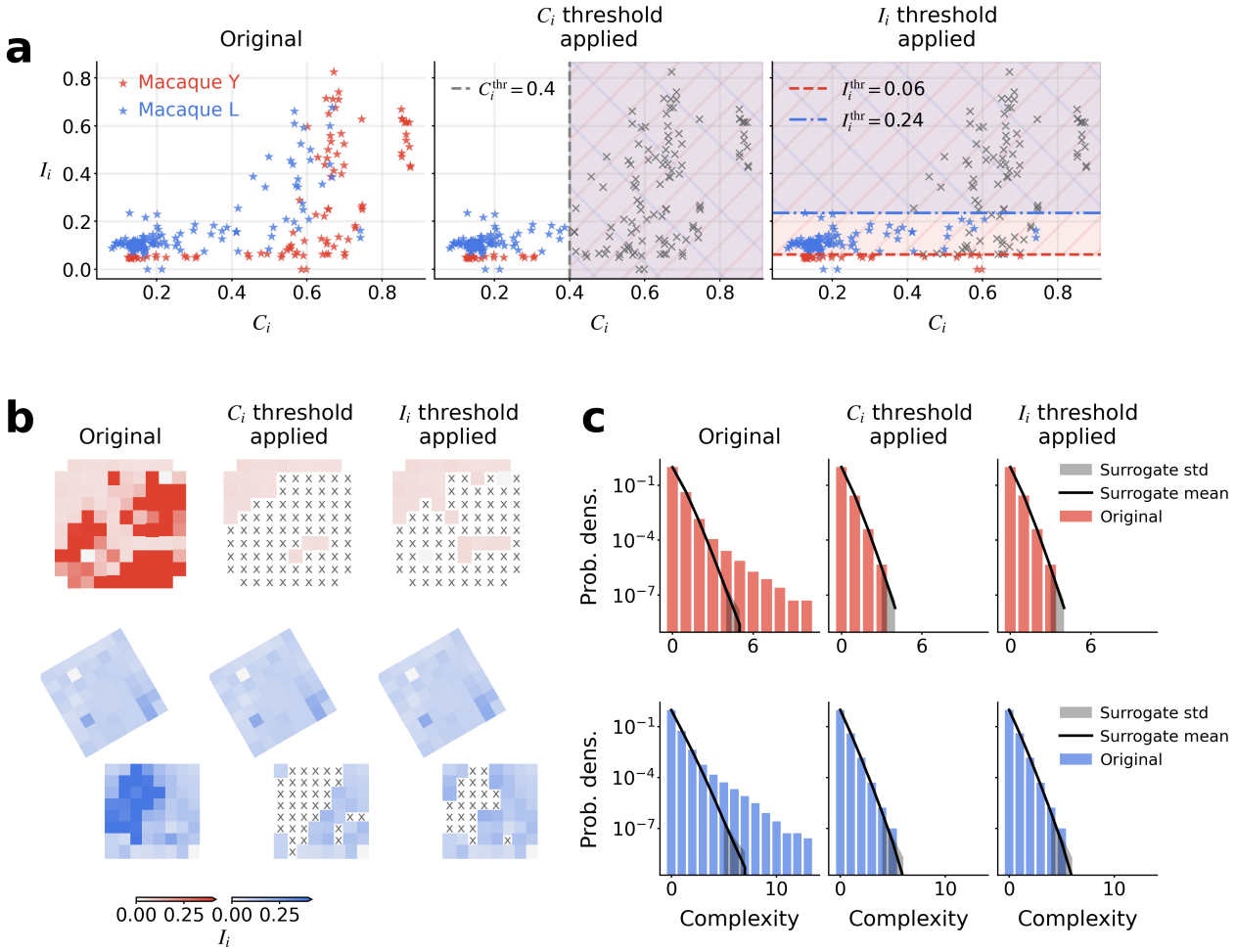

Figure 5: Synchrofact removal based on channel screening. a) The channel-wise highest correlation coefficient C_i (x-axis) vs. the global HSE index I_i (y-axis) for channel i. (Left) C_i vs. I_i calculated using all channels. (Middle) Recalculated using only channels with a C_i lower than 0.4. (Right) Recalculated using only channels with a low I_i. b) Channels excluded by the proposed methods, shown on the electrode grid of the arrays. Crosses indicate the excluded channels. Colors indicate the I_i values of the remaining channels. c) Complexity distribution for the channels remaining after the two channel screening methods (middle and right), compared to the original (left, calculated as in Synchronous spike events are ubiquitous in multi-electrode systems).

Synchrofacts can remain in spike sorted data

We then also consider the case with sorted SUA spikes. In this case, the model indicates that, if the spike sorting is perfect, the HSE index for a SUA pair must be either 1 or a very small value reflecting chance coincidences. If this is the case, that would make the screening of SUAs for synchrofact removal almost trivial. Here we investigate whether this really applies to experimental data, using semi-manually sorted data of macaque Y (see Spike Sorting in STAR Methods for the spike sorting procedure). One needs to note here that the spike sorter used for this data set (Plexon Offline Sorter, version 3.3.3) has a functionality to reject cross-channel artifacts, which marks spike-like events that occur simultaneously on a defined percentage of channels (70%) as "invalidated waveforms" (see Spike Sorting in STAR Methods). Thus, HSEs with extremely high complexities, which can be caused by common noise artifact (an extreme example is shown in Supplementary Figure S4), had already been removed by the sorter. However, pairwise or group-wise correlations that are expected from cross-talk might go unnoticed, since spike sorting was done independently per channel and hence the similarity of waveforms and/or spike times between channels cannot be noticed during the process. Additionally, to ensure the quality of the spike trains after spike sorting, typically a number of quality metrics are used to filter SUAs. Here we require the waveform signal-to-noise ratio to be larger than 2.5, and reject SUAs with an average firing rate $< 1\,\mathrm{Hz}$.

In the following we perform the same analysis as for the MUA data, but now on pairs of SUAs. We compute the pairwise HSE index $I_{i,j}$ as before (see Measure of spike synchrony in STAR Methods), with the subscripts i and j here denoting different SUAs rather than channels. Figure 6a shows $I_{i,j}$ for SUA pairs plotted against the raw signal correlation coefficient $c_{i,j}$ for the channels that the respective SUAs belong to. Similar to the results from channel pairs (c.f. Figure 3e, left), the $I_{i,j}$ values increase with increasing $c_{i,j}$ values, with a sharp increase after $c_{i,j} \sim 0.4$ taking values between 0 and 1. This spread of $I_{i,j}$ values between 0 and 1 is contradictory to the model prediction for the case of perfect spike sorting. Thus, in the SUA pairs with intermediate $I_{i,j}$ values between 0 and 1, the respective SUAs should include spikes from different neurons, which were not separated by the spike sorting.

Those SUAs that are contaminated by cross-talk should be removed from analyses, since they do not faithfully represent the activity of a single neuron and hence would hamper correct interpretation of respective analysis results. In a similar manner to the channel screening in the previous section (see Channel removal for synchrofact mitigation in Results), we can consider a screening of SUAs based on the global HSE index computed for SUAs and the respective channel-wise highest raw signal correlation coefficient. The global HSE index I_i for SUA i is calculated in the same way as for a channel (equation (2)), i.e., now as the ratio of the number of SUA i spikes participating in HSEs to the total number of of the SUA i spikes. Figure 6b shows I_i for SUAs plotted against their respective C_i. One can screen SUAs based on this plot, either by setting a threshold on C_i or on I_i. As shown in the complexity distribution (Figure 6c), we obtain similar results as we got for MUAs: excluding the worst SUAs removes most of the synchrofacts from the data set. Thus, the proposed method remains valid and necessary for spike sorted data.

Impact of synchrofacts on data analysis

Synchrofacts that remain unnoticed in the data can affect the results and interpretation of various analyses. To illustrate the danger of undetected synchofacts, we demonstrate their impact on two types of analyses.

First, we show that synchrofacts can significantly alter the estimation of neuronal tuning curves. We simulate spike trains of motor cortex neurons with a hand movement direction preference (Georgopoulos et al., 1982). The neurons modulate their firing rates in a sinusoidal manner as a function of the direction of the hand movement: the highest firing rate occurring at the preferred hand movement direction. Here, we consider a pair of neurons with different preferred directions (PDs), mean firing rates (FRs), and rate-modulation depths (MDs). We assume that these neurons are recorded in two separate channels, cross-talking with strength α, such that one channel (referred to as the source channel) provides artifact spikes to the other channel (referred to as the target

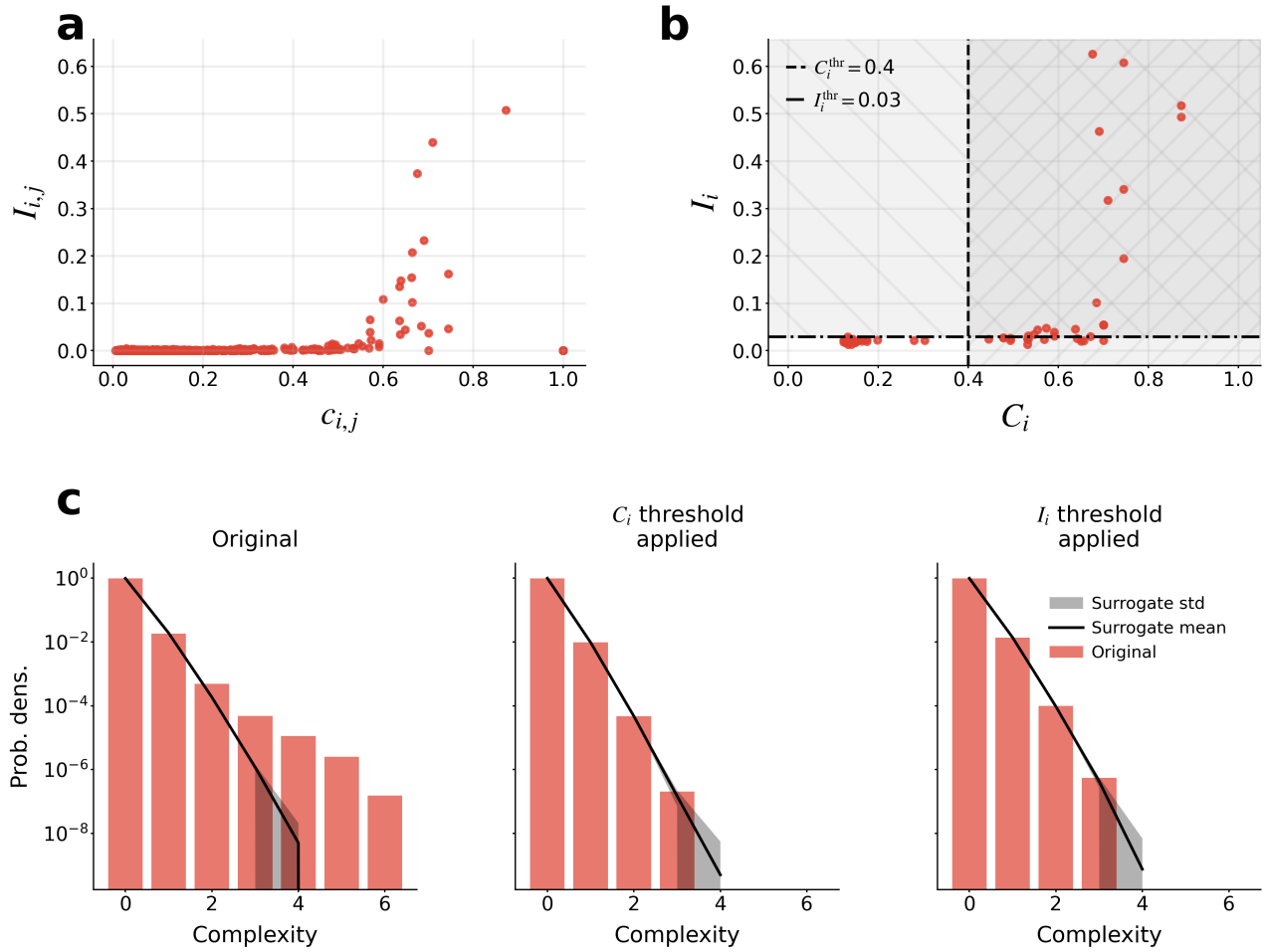

Figure 6: Detection and removal of synchrofacts in spike sorted data from macaque Y. (a) Pairwise HSE index $I_{i,j}$ for SUA pairs vs. raw signal correlation $c_{i,j}$ of the respective channel pairs. Note that SUA pairs on an identical channel always yield $(c_{i,j}, I_{i,j}) = (1, 0)$. (b) Global HSE index I_i of SUA i vs. the channel-wise highest raw signal correlation coefficient C_i of the corresponding channel. The vertical and horizontal lines indicate the threshold for C_i and I_i, respectively, used for removal of SUAs with the proposed method. (c) Complexity distribution computed from the spike sorted data, (left) the original data, (middle) data after SUA removal with the C_i thresholding method, (right) data after SUA removal based on the I_i thresholding method.

channel). The neurons in the source and target channel are referred to as the source neuron and the target neuron, respectively.

With this setup, we examine how the tuning curve estimated from the spike train in the target channel is modulated by the artifact spikes from the source channel (Figure 7a). We consider various levels of cross-talk strength α and their impact on the estimated tuning curve (gray curves in Figure 7a). The three examples in Figure 7a illustrate cases with different combinations of FRs, MDs, and PDs of the two neurons. In Figure 7a (left), the target and source neuron have PDs of 180° (blue curve) and 90° (orange curve), respectively, and both have the same FR and MD. With increasing cross-talk strength, the FR and the MD of the estimated tuning curve gets larger, and in particular, the peak of the estimated tuning curve shifts closer to the source PD. Figure 7a (center) shows a similar example, where the target neuron has a lower FR and smaller MD than the source neuron, while the PDs of both neurons are unchanged. As in the first case, the estimated tuning curve changes with increasing α, but here it reaches a much higher similarity to the source tuning, due to the higher FR of the source neuron than the target neuron. In Figure 7a (right), the two PDs are opposite: the target at 180° and the source at 0°. Due to the high FR and large MD of the source neuron, the estimated PD becomes more and more similar to the source PD with increasing α, switching the PD by 180°, and its FR becomes much higher than the original target neuron. From these examples we conclude that any of the PD, FR, and MD of the tuning can be considerably altered by the cross-talk. High firing rate does not protect a neuron from the impact of cross-talk. Thus, cross-talk can fully alter the result from tuning curve estimations, leading to false results.

Another example of the impact of synchronfacts is on the analyses for excess spike synchrony using Unitary Event (UE) analysis, as explained in Unitary Event analysis in STAR Methods. UE analysis (Grün et al., 2002a,b; Grün & Rotter, 2010) detects excess spike synchrony in a simultaneously recorded pair of spike trains by computing the empirical and expected number of spike coincidences. Here we consider a pair of independent Poisson spike trains (10 spikes/s, 5 s duration) as the ground truth spike signals of a pair of channels, and examine how the cross-talk between these channels affects the result of the UE analysis. According to our model, the empirical number n_{emp} of spike coincidences is obtained as $n_{1,2}$ derived in Subsection Cross-talk model explains the emergence of synchrofacts, while the expected number n_{exp} is calculated from the firing rates of the measured spike trains. Figure 7b (left) shows the difference between n_{emp} and n_{exp} as a function of raw signal correlation $c_{i,j}$ between the two channels, for a range of the ground truth spike amplitude r^{SN}. The larger the $c_{i,j}$ value (due to the stronger cross-talk), the more spikes bleed across channels (see Cross-talk model explains the emergence of synchrofacts in Results) and thus more synchrofacts are generated, resulting in the increased difference between n_{emp} and n_{exp}. This effect is stronger with larger spike amplitude r^{SN}. As a consequence, for large $c_{i,j}$ values, the significance of the difference (Figure 7b, right), expressed here as the surprise (see Unitary Event analysis in STAR Methods), rises beyond the 5% significance level. The larger the spike amplitude r^{SN}, the lower the value of $c_{i,j}$ at which the surprise crosses the significance threshold. This result shows that, if cross-talk goes unnoticed, the data may be wrongly found to contain significantly excess spike synchrony. This will also happen when the data are binned at larger bin sizes, e.g. 1 ms or more. By excluding channels as proposed here to remove artifacts one can avoid such false positive results.

These are just two examples showing the impact of synchrofacts, but other types of analysis would also be similarly affected and could also produce wrong results in the presence of synchrofacts. To avoid false results, we encourage researchers to make considerable efforts to remove synchrofacts from their data.

Discussion

We have shown, based on examination of electrophysiological recordings from multiple laboratories, that HSEs in massively parallel spike trains commonly contain synchrofacts, i.e., artifactual extremely precise (at the data sampling resolution) spike synchrony events. Synchrofacts express themselves in the raw signal as nearly identical activity traces, observed in distant electrodes with submillisecond precision, strongly suggesting that they originate

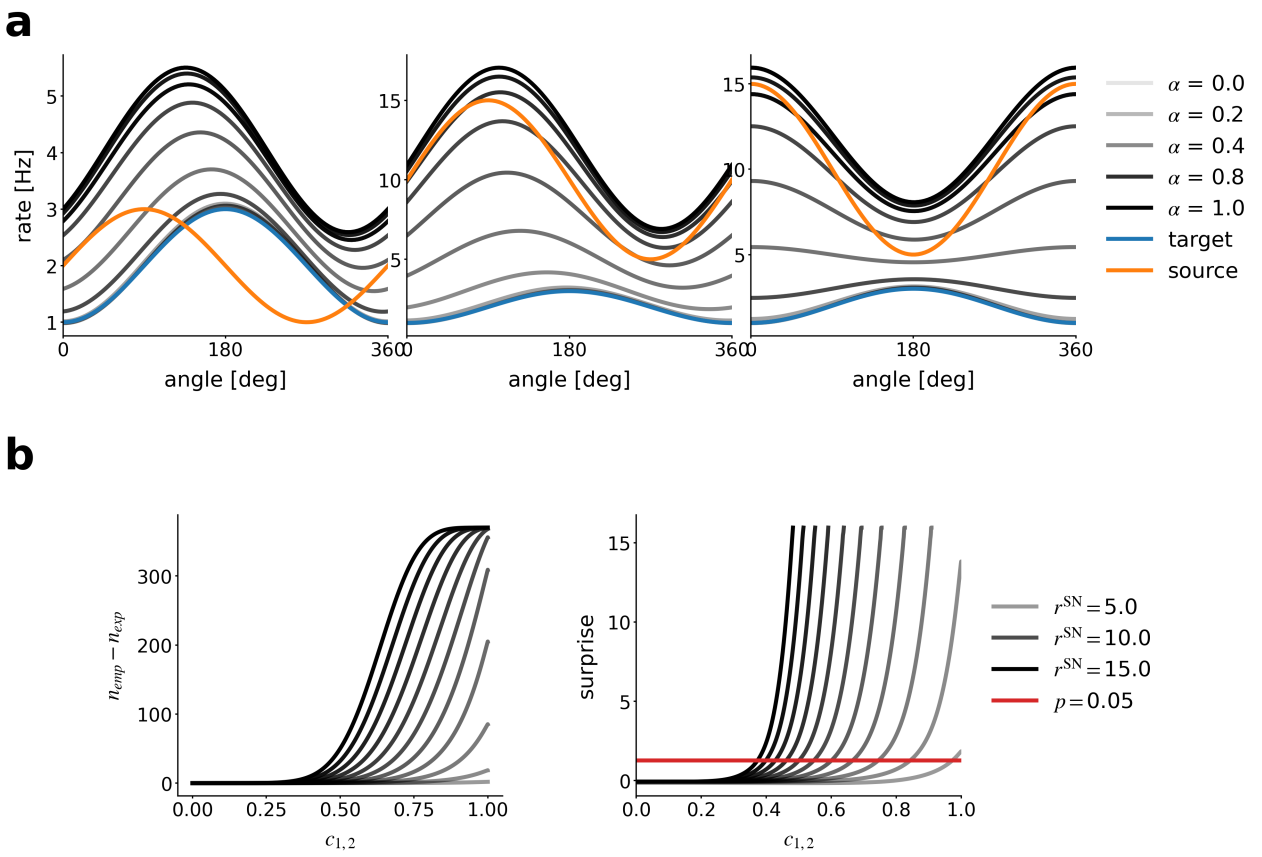

Figure 7: Impact of synchrofacts on data analyses. (a) Impact on neuronal tuning, for three example cases with different combinations of target and source neuron's tuning properties. The tuning curves of the target and source neuron are shown by blue and orange curves, respectively. The tuning curve estimated from the spike trains measured in the target channel is shown in gray, with different shades according to the cross-talk strength α as indicated in the legend to the right. (b) Impact on Unitary Event analysis. Left: excess spike synchrony, measured as the difference between the empirical and expected number of synchronous spike events, as a function of raw signal correlation. Right: surprise of the excess synchrony as a function of raw signal correlation. The surprise value corresponding to the 5% significance level is indicated by the red horizontal line. In both plots, results for different values of spike amplitude r^{SN} are shown in different shades of gray.

from external noise or cross-talk in the recording hardware. We introduced a new measure, the HSE index ($I_{i,j}$), to quantify the occurrences of HSEs in each channel pair, and showed its systematic relation to the correlation coefficient ($c_{i,j}$) of the band-pass filtered raw signals. We also presented a minimal model of cross-talking signals that explains the observed relation between $I_{i,j}$ and $c_{i,j}$, suggesting that cross-talk is the main source for the synchrofacts. Based on the observations and the model, we suggested excluding particularly affected channels by thresholding either $I_{i,j}$ or $c_{i,j}$, which removes nearly all above-chance HSEs. We also showed that spike sorting alone does not necessarily remove synchrofacts and further filtering is still required. We thus highlighted the importance of removing these artifacts from neural data, since they could bias analyses and produce misleading results.

As a first step to mitigate artifacts, we tried to identify their physical sources in the experimental recording setup. We found many short lived artifacts associated with external events such as switching on a light or closing of a door. Unfortunately, it was not feasible to construct a Faraday cage around the recording setup to avoid external electromagnetic waves. Cross-talk was another potential source of artifacts, which had been known to happen between electrode shanks at relatively short distances (Nelson et al., 2017). Since we observed artifacts at large distances Figure 2, we searched for alternative locations of the cross-talk. Since the placement of the individual channels in the connector to the head stage does not seem to explain the cross-talk Figure S2, the circuitry inside the headstage is our primary suspect for cross-talk. There the analog signals from many channels are simultaneously amplified, filtered and converted to digital; steps known to be very sensitive to cross-talk (Pérez-Prieto & Delgado-Restituto, 2021; Perez-Prieto et al., 2021). Indeed, in the case of macaque Y, previous recordings had used the analog signal processing headstage 'Samtec' and 'Patientcable' (Blackrock Microsystems) (Riehle et al., 2013; Brochier et al., 2018), and after updating it to 'Cereplex E' (Blackrock Microsystems) we observed far fewer artifacts, likely due to the improved insulation and circuit design. In the case of macaque L 'Cereplex M' (Blackrock Microsystems) was used. Since it was not possible to determine the sources of cross-talk, we developed the post-hoc artifact removal methods presented in this paper.

We have suggested two approaches to remove synchrofacts: applying a threshold on the channel-wise maximum correlation C_i of the raw signals , or a threshold on the global HSE index I_i. Applying the C_i threshold excludes slightly more channels than the I_i threshold. We advise using the C_i threshold because the remaining channels better agree with the chance distribution of HSEs. Which approach to take depends on the planned analysis and its sensibility to precise spike correlations.

The complete removal of the HSEs with complexities > 1 on the 1/30 ms timescale can damage the data, since the lack of chance synchrony (see Figure S1) can be noticed even on longer timescales on the order of several ms. As a result, potentially existing neuronal spike synchrony may be undetected (Oberste-Frielinghaus, 2022). A previous study (Torre et al., 2016) removed all HSEs with complexities ≥ 2. This led to an underestimation of the chance synchrony in the data (see Figure S1). While the study has already revealed a particular organization of synchronous spike patterns, re-examination of the same data with our new synchrofact removal method might lead to stronger and clearer results.

A previous study (Chen et al., 2022) defined a 'synchrofact participation' (SP) ratio as the number of synchronous spike events above chance, derived by a bootstrap method on the complexity distribution. The channels with highest SP were removed iteratively, which re-evaluates the chance levels after removing each channel. This iterative approach is less strict than ours, in the sense that, when two channels have strong cross-talk, only removing one of them will avoid above-chance synchrony. However, some of the spikes detected in the remaining channel could actually originate from the removed channel, and hence the physical location of the neurons becomes unclear. To avoid such ambiguities we did not employ such an iterative approach here, opting to remove both contaminated channels.

An obvious idea is that false 'spikes' are filtered out by spike sorting, since it involves multiple filtering steps that would reject spurious spikes. However, following our model, the cross-talk copies spikes into other channels without major distortions to the waveform, and therefore the copied spikes cannot be readily distinguished from

real spikes. In fact, in a former study (not shown here) we tried to discriminate between real spikes and artifact spikes by cross-correlating spike waveforms, but it was not successful. Here we found that also in spike sorted data synchrofacts are present, demonstrating that spike sorting does not completely remove artifacts (Figure 6, Figure S3). However, spike sorted data does show less artifacts than unsorted data, so spike sorting somewhat reduces the problem.

In this work we only showed data recorded with hardware from the same manufacturer, which raises the question whether recordings using other electrodes, such as high-density Neuropixels probes, may be less affected by such artifacts. Neuropixels record individual neurons on more than a single recording site, since they are very close (40 μm) to each other. This enables spike sorting that takes into consideration more than one signal per neuron, e.g. by using the Kilosort sorter (Steinmetz et al., 2021; Pachitariu et al., 2023). Nevertheless, we also found above-chance HSEs in Neuropixels recordings (Jain et al., 2022), highlighting the ubiquity of artifacts and the importance of adequate postprocessing methods.

In summary, we showed that synchrofacts are ubiquitous in multi-electrode recordings and are likely caused by cross-talk in the recording system. We suggest to compare the complexity distribution of the data with surrogate data at the data sampling resolution for indications of artifacts. The approach we proposed here to remove synchrofacts requires access to the original broadband signal at data sampling resolution. This enables us to relate the pairwise coincidence of spike-like events to the raw signal correlation, and remove the most affected channels. In our data, cross-talk was the primary source of synchrofacts, and our proposed method effectively removed the synchrofacts by excluding the most affected channels. If higher-than-chance complexity events remain after the channel exclusion, artifacts originating from common external noise may be present and should also be removed by excluding the affected time periods from further analysis. Synchrofacts are ubiquitous in multi-electrode neural recordings and their presence can affect various analyses. Therefore detection and removal of synchrofacts is crucial for avoiding false results and ensuring a sound interpretation of the obtained results.

STAR Methods

RESOURCE AVAILABILITY

Lead contact

Further information and requests for resources should be directed to and will be fulfilled by the lead contact, Jonas Oberste-Frielinghaus (j.oberste-frielinghaus@fz-juelich.de).

Materials availability

This study did not generate new unique reagents.

Data and code availability

The electrophysiology data from macaque L were previously published and are publicly accessible (Chen et al., 2022). The electrophysiology data for macaque Y, together with all processed data for this project (threshold crossings, cross-correlation, HSE index etc.) have been deposited in a GIN repository and are publicly available at the time of publication under a Creative Commons Attribution-ShareAlike 4.0 International Public License. The DOI to the repository is listed in the key resources table. All original code has been deposited at the same GIN repository and is publicly available as of the date of publication. Any additional information required to reanalyze the data reported in this paper is available from the lead contact upon request.

EXPERIMENTAL MODEL AND STUDY PARTICIPANT DETAILS

Macaques

We analyzed the resting state data from two (N=2) rhesus macaques (*Macaca mulatta*), recorded in two different experimental laboratories. The data from macaque L was collected at the Netherlands Institute for Neuroscience, and previously published (Chen et al., 2022). The data from macaque Y was collected at the Institut de Neurosciences de la Timone, with the recording apparatus described by de Haan et al. (2018). At the time of the array implantation macaque L (male) was 7 years old and weighed ~ 11 kg; and macaque Y (female) was 6 years old and weighed ~ 7 kg. All experimental and surgical procedures for macaque L complied with the NIH Guide for Care and Use of Laboratory Animals, and were approved by the institutional animal care and use committee of the Royal Netherlands Academy of Arts and Sciences (approval number AVD-8010020171046). All experimental and surgical procedures for macaque Y were approved by the local ethical committee (C2EA 71; authorization Apafis#13894-2018030217116218v4) and conformed to the European and French government regulations.

METHOD DETAILS

Data collection

Both macaques were recorded using setups based on the Blackrock Microsystems ecosystem.

Macaque L See Chen et al. (2022) for an in-depth description of this data set. Briefly, electrophysiological signals originating from the V1 and V4 regions were recorded using a configuration of 1024 channels distributed across 16 Utah Arrays, each comprising 8x8 electrodes. Sampling was performed at a rate of 30 kHz. The signal pathway commenced with the passive conduction of neuronal signals from the 1024-channel pedestal to an Electronic Interface Board (EIB). This EIB was equipped with 32 36-channel Omnetics connectors, facilitating the interface with eight 128-channel CerePlex M headstages. The CerePlex M headstages applied a 0.3–7500 Hz analog filter at unity gain, refraining from signal amplification. Analog-to-digital conversion (ADC) was conducted by the CerePlex M, employing a 16-bit resolution with a sensitivity of 250 nV/bit. The digitized signal was subsequently routed to a 128-channel Digital Hub, with each Digital Hub processing data originating from one CerePlex M, which in turn was linked to two electrode arrays. The Digital Hub undertook the conversion of the digital signal into an optic-digital format. This transformed signal was then transmitted via an optic-fiber cable to a 128-channel Neural Signal Processor (NSP) for subsequent processing and storage. Each Digital Hub supplied the signal to a single NSP. In total, eight NSPs were employed, with each NSP managing data derived from two electrode arrays. In the present study, we focused on a single data stream (NSP1) from one session, which included one array in V1 and one array in V4. These arrays showed many synchrofacts in a previous less exhaustive analysis (Chen et al., 2022), including events across both arrays, even though they were separated by the lunate sulcus. Thus, this data stream was particularly useful to demonstrate the non-neural origin of the synchrofacts. We manually found a large artifact event (see Common noise artifact example) which we cut out before the analysis of the data.

Macaque Y Electrophysiological signals originating from V1, V2, DP, and 7A were recorded with four separate 6x6-electrode Utah Arrays. Additionally, M1/PMd was recorded with a 10x10-electrode Utah Array. Sampling was performed at a rate of 30 kHz. In contrast to monkey L, the signal pathway commenced with two 128-channel pedestals (CerePort): One for the four 36-channel arrays and one for the 100-channel array. Each of the pedestals interfaced with a 128-channel CerePlex E headstage. Notably, the CerePlex E headstages applied a 0.3–7500 Hz analog filter at unity gain, refraining from signal amplification. Analog-to-digital conversion (ADC) was conducted by the CerePlex E, employing a 16-bit resolution with a sensitivity of 250 nV/bit. The digitized signal

was subsequently routed to a 128-channel Digital Hub, with each Digital Hub processing data originating from one CerePlex E, which in turn was linked to one 100-channel array or four 36-channel arrays. The Digital Hub undertook the conversion of the digital signal into an optic-digital format. This transformed signal was then transmitted via an optic-fiber cable to a 128-channel Neural Signal Processor (NSP) for subsequent processing and storage. Each Digital Hub supplied the signal to a single NSP. In total, two NSPs were employed. In the present study, we focused on the M1/PMd array from one session, to demonstrate that synchrofacts are not limited to visual processing areas.

Signal processing and threshold crossings

All offline signal processing steps (except for spike sorting) and data analysis described below were performed by original custom codes written in the Python programming language and executed in a pipeline defined as a Snakemake workflow (Mölder et al., 2021). The recorded raw signals were band-pass filtered in the frequency range of 250 Hz − 7500 Hz (a second order Butterworth filter, as implemented in the `signal_processing.butter()` function in the Elephant toolbox (Denker et al., 2018)). According to Quiroga (2007), putative spikes were extracted from the high-pass filtered raw signal of each channel by thresholding it at

$$\text{Threshold} = -5 \cdot \text{median}\left(\frac{|s_i|}{0.6745}\right),$$

where s_i denotes the high-pass filtered raw signal of channel i. The time of threshold crossing of each putative spike was registered as the time of that spike. The resulting spike times per channel were taken as the spike train of the multi-unit activity of that channel.

Spike Sorting

Spike sorting was performed only on the macaque Y data. Details of the sorting procedure are described by Brochier et al. (2018). The spike waveforms which were extracted and saved during the recording were offline sorted using the Plexon Offline Sorter (version 3.3.3). We started by merging all online extracted waveforms back into one pool per channel and marking them as "unsorted waveforms" in the Plexon Offline Sorter. For the invalidation of cross-channel artifacts (e.g., chewing artifacts), all waveforms that occurred simultaneously on a defined percentage of channels (70%) were then marked as "invalidated waveforms" in the Plexon Offline Sorter. Furthermore, a waveform rejection was performed. Thereby all waveforms of abnormally large amplitude and/or atypical shape on a channel were manually also marked as "invalidated waveforms" in the Plexon Offline Sorter. The actual spike sorting was then performed on the remaining unsorted waveforms (i.e., those not marked as invalidated waveforms) individually for each channel. We used different algorithms to split these waveforms into clusters in a 2- or 3-dimensional principal component (PC) space. The dimensionality of the PC space was chosen according to the best separation. The main algorithms used were K-Means(-Scan) and Valley Seeking (chosen according to the best separation). We used a fixed threshold for outliers (a parameter to be determined in the Plexon Offline Sorter) between 1.8 (K-Means) and 2 (Valley Seeking) to get comparable sorting results. The spikes of the sorted clusters were then controlled using the inter-spike interval (ISI) distributions and the auto- and cross-correlation plots. Clusters with unacceptable outcomes (completely or partly overlapping waveforms), including those with only a few spikes, were left assigned as "unsorted waveforms" in the Plexon Offline Sorter.

Cross-talk model

Electric cross-talk between channels and its influence on the signals are modeled as follows. First, we consider the "ground truth" signals (i.e., not contaminated by cross-talk) $x_1(t_i)$ and $x_2(t_i)$ for channel 1 and 2, respectively, where t_i $(i = 1, 2, 3, ...)$ are discrete sampling times. For simplicity, we assume that x_1 and x_2 are time

series of independent Gaussian white noise with the same mean $E[x_1] = E[x_2] = 0$ and the same variance $\mathrm{Var}(x_1) = \mathrm{Var}(x_2) = \sigma^2$.

Next, we model the cross-talk as a linear mixing of these two signals. Concretely, we define the measured signals $s_1(t_i)$ and $s_2(t_i)$ for channel 1 and 2, respectively, as:

$$\begin{aligned} s_1 &= x_1 + \alpha x_2 \\ s_2 &= x_2 + \alpha x_1, \end{aligned}$$

where α is a parameter representing the strength of the cross-talk: s_1 and s_2 are identical when $\alpha = 1$, and they are independent when $\alpha = 0$. By this construction, both s_1 and s_2 obey a Gaussian distribution with the mean $E[s_1] = E[s_2] = 0$ and the variance $\mathrm{Var}(s_1) = \mathrm{Var}(s_2) = (1+\alpha^2)\sigma^2$. The Pearson correlation coefficient c_{12} for the signals s_1 and s_2 is derived as:

$$\begin{aligned} c_{12} &= E\left[s_1 s_2\right] / \left(\sqrt{E\left[s_1^2\right]}\sqrt{E\left[s_2^2\right]}\right) \\ &= E\left[\left(x_1 + \alpha x_2\right)\left(x_2 + \alpha x_1\right)\right] / \left(\sqrt{E\left[\left(x_1 + \alpha x_2\right)^2\right]}\sqrt{E\left[\left(x_2 + \alpha x_1\right)^2\right]}\right) \\ &= 2\alpha\sigma^2 / \left(\sqrt{\left(1+\alpha^2\right)\sigma^2}\sqrt{\left(1+\alpha^2\right)\sigma^2}\right) \\ &= = 2\alpha / \left(1+\alpha^2\right). \end{aligned}$$

We further introduce spikes to the signals. Here we model spikes in channel 1 by adding a value A_1, representing the spike amplitude, to x_1 at various, random time points. We parameterize A_1 as $A = \sigma r_1^{\mathrm{SN}}$, where r_1^{SN} is the signal-to-noise ratio of the spike waveform, such that SUAs with different spike amplitudes are represented by modifying the value of r_1^{SN}. The spikes introduced in the ground truth signal x_1 are transferred to the measured signals s_1 and s_2 via the cross-talk. To count those transferred spikes, we extract spikes from s_1 by thresholding it at $m\sigma_{s_1}$, where $\sigma_{s_1} = \sqrt{1+\alpha^2}\sigma$ is the standard deviation of s_1 and m is a multiplier determining the threshold in relation to the standard deviation. Assuming that N_1 spikes were introduced to x_1, we can derive the expected number n_{11} of the spikes transferred from x_1 and detected in s_1 ($= x_1 + \sigma r_1^{\mathrm{SN}} + \alpha x_2$ at spike times) as:

$$\begin{aligned} n_{11} &= N_1 \cdot P\left(x_1 + \sigma r_1^{\mathrm{SN}} + \alpha x_2 > m\sigma_{s_1}\right) \\ &= N_1 \cdot P\left(x_1 + \alpha x_2 > \left(\sqrt{1+\alpha^2}m - r_1^{\mathrm{SN}}\right)\sigma\right) \\ &= N_1 \cdot P\left(\mathcal{N}\left(0, \left(1+\alpha^2\right)\sigma^2\right) > \left(\sqrt{1+\alpha^2}m - r_1^{\mathrm{SN}}\right)\sigma\right) \\ &= N_1 \cdot P\left(\mathcal{N}\left(0,1\right) > m - r_1^{\mathrm{SN}}/\sqrt{1+\alpha^2}\right) \\ &= N_1 \cdot \mathrm{erfc}\left(\left(m - r_1^{\mathrm{SN}}/\sqrt{1+\alpha^2}\right)/\sqrt{2}\right)/2, \end{aligned}$$

where $\mathrm{erfc}(\cdot)$ is the complementary error function. [1]

Note that the factor $p_{11} \equiv \mathrm{erfc}\left(\left(m - r_1^{\mathrm{SN}}/\sqrt{1+\alpha^2}\right)/\sqrt{2}\right)/2$ in front of N_1 in the above expression represents the probability that a spike transferred from the ground truth signal x_1 is detected in the measured signal s_1. In a similar manner, the probability p_{21} that a spike originally in x_1 is detected in s_2 is derived as $\mathrm{p}_{21} = \mathrm{erfc}\left(\left(m - \alpha r_1^{\mathrm{SN}}/\sqrt{1+\alpha^2}\right)/\sqrt{2}\right)/2$. Furthermore, assuming N_2 spikes in the other ground truth signal x_2, the probabilities p_{12} and p_{22} that those spikes are detected in the measured signals s_1 and s_2, respectively, are derived as $p_{12} = \mathrm{erfc}\left(\left(m - \alpha r_2^{\mathrm{SN}}/\sqrt{1+\alpha^2}\right)/\sqrt{2}\right)/2$ and $p_{22} = \mathrm{erfc}\left(\left(m - r_2^{\mathrm{SN}}/\sqrt{1+\alpha^2}\right)/\sqrt{2}\right)/2$.

With these probability values, the expected numbers n_1 and n_2 of spikes detected in the measured signals s_1

[1] Note that, for simplicity, this formalism does not consider "noise" spikes which arise from the random fluctuations of the background signal that happen to cross the threshold by chance.

and s_2, respectively, are represented as:

$$\begin{aligned} n_1 &= p_{11}N_1 + p_{12}N_2 \\ n_2 &= p_{21}N_1 + p_{22}N_2, \end{aligned}$$

given the numbers N_1 and N_2 of spikes in the ground truth signals x_1 and x_2, respectively. Note that the terms $p_{12}N_2$ and $p_{21}N_1$ represent the number of spikes transferred from the other channel, and hence these spikes are detected in the both of the measured signals. Thus, the sum of these terms: $n_{1,2} = p_{12}N_2 + p_{21}N_1$ represents the number of synchrofacts in this pair of measured signals. Using this, the HSE index $I_{1,2}$ between the measured signals s_1 and s_2 (synchrofact index) is expressed as:

$$I_{1,2} = \begin{cases} n_{1,2}/n_1 = (p_{12}N_2 + p_{21}N_1) \,/\, (p_{11}N_1 + p_{12}N_2) & (n_1 \leq n_2) \\ n_{1,2}/n_2 = (p_{12}N_2 + p_{21}N_1) \,/\, (p_{21}N_1 + p_{22}N_2) & (n_1 > n_2) \end{cases},$$

which takes a value between 0 and 1 depending on the parameters.

QUANTIFICATION AND STATISTICAL ANALYSIS

Complexity and estimation of chance levels

To study fine-temporal correlation and detect potential synchronous artifacts in parallel spike train data, we first bin the time axis of the spike trains with a predefined bin width (in the present study we use 1, 0.1, and 1/30 ms bin widths) and compute the complexity of spiking activity at each bin, i.e., the number of units contributing spikes to that bin. Then we make a histogram of the complexity values for all the bins throughout the recording, called complexity distribution (Grün et al., 2008). For easier comparison of the results from different data sets, the histogram is normalized by dividing the counts of all complexities (including the complexity of zero, i.e., bins with no spikes) by the total number of bins, such that the sum of the histogram values over all complexities equals to unity.

We compare the empirical distribution to chance levels from independent data, to elucidate if the real data contains excess spike synchrony. To estimate the complexity distribution of independent data, we use surrogate data, i.e., modified versions of the original data where spike times are intentionally altered. Stella et al. (2022) compared a number of surrogate methods, and according to that, we employ here the 'time-shift' method (with a 30 ms shift width, (Pipa et al., 2008)), by which the spike trains are randomly shifted in time against each other. Time shifting destroys potential correlations between spike trains, while conserving many other features of the data such as the inter-spike interval distribution, the firing rate modulations and autocorrelation (Stella et al., 2022). We generate 200 surrogate spike train data sets, and for each of them we compute the complexity distribution. The mean and standard deviation of the count are calculated for each complexity, and plotted together with the empirical complexity distribution for comparison.

Cross-correlation of high-pass filtered raw signals

The correlation c_{ij} between the raw signals of channel i and j is evaluated by the Pearson correlation coefficient as:

$$c_{i,j} = \frac{\mathrm{Cov}(s_i, s_j)}{\sqrt{\mathrm{Var}(s_i)\mathrm{Var}(s_j)}},$$

where s_i and s_j represent the high-pass filtered raw signals of channel i and j, respectively, obtained as described in Signal processing and threshold crossings, and $\mathrm{Var}(s_i)$ and $\mathrm{Cov}(s_i, s_j)$ represent the variance of s_i and the covariance between s_i and s_j, respectively.

Measure of spike synchrony

Assume that we have n_i spikes in channel i at times t_i^p $(1 \le p \le n_i)$. We discretize the time axis in bins of width b, which should be small enough to contain at most one spike in a bin, and obtain a set of bin indices $T_i = \{\tau_i^p | 1 \le p \le n_i\}$, which indicates the positions of the time bins where the spikes are observed (in other words, the time of the p-th spike is in the time range $(\tau_i^p b, (\tau_i^p + 1)\, b)$). The number $n_{i,j}$ of spike synchrony events between channels i and j is obtained as $n_{i,j} = |T_i \cap T_j|$. We define the pairwise HSE index $I_{i,j}$ as

$$I_{i,j} = \frac{n_{i,j}}{\min(n_i, n_j)},$$

which is a measure of the abundance of spike synchrony events between a pair of channels i and j. We choose to divide by the smaller spike count so that the HSE index is independent of the channel order (i.e., $I_{i,j} = I_{j,i}$) and also sensitive to HSEs occurring on channels with small number of spikes.

In a similar manner, we define the global HSE index I_i as

$$I_i = \frac{n_{i,\bar{i}}}{n_i},$$

where $n_{i,\bar{i}}$ is defined as $n_{i,\bar{i}} = |T_i \cap \bigcup_{j \neq i} T_j|$, which represents the number of spike synchrony events between channel i and any other channel. Thus, the global HSE is a measure of the abundance of spike synchrony events between channel i and any other channel.

Unitary Event analysis

Unitary Event analysis (Grün et al., 2002a,b; Grün & Rotter, 2010) is a statistical method which enables to derive excess spike synchrony from a simultaneously recorded pair of spike trains. The method computes the empirical and the expected number of synchronous spike events and evaluates the statistical significance of the difference between the two. Suppose that we have two simultaneously recorded spike trains of duration T. We bin the time with a bin width of b and count spikes of each spike train (if multiple spikes are in a bin, the count is clipped to 1). Then we count the empirical number n_{emp} of spike coincidences by counting the number of filled bins at the same times in both spike trains. Next, we compute the expected number n_{exp} of spike coincidences in the following steps: 1) estimate the spiking probabilities p_1 and p_2 for the two spike trains, by dividing the total number of spikes in each spike train by the total number of the bins (i.e., T/b). 2) estimate the probability of spike coincidence in a bin as $p_1 p_2$, by assuming independence of the spike times of the two spike trains. 3) obtain the expected number n_{exp} of spike coincidences by multiplying the coincidence probability by the total number of bins, i.e., $n_{\mathrm{exp}} = p_1 p_2 T/b$. If the spike trains obey the Poisson statistics, the spike coincidence count should obey a Poisson distribution of the mean n_{exp}. Hence, the p-value of the empirical coincidence count n_{emp} can be derived (under the null-hypothesis of Poisson spike trains) as $p = \Sigma_{n=n_{\mathrm{emp}}}^{\infty} P_{\mathrm{poisson}}(n|n_{\mathrm{exp}})$. The significance of the p-value is quantified by the joint surprise S defined as $S = \log_{10}(1-p)/p$.

KEY RESOURCES TABLE

REAGENT or RESOURCE	SOURCE	IDENTIFIER
Experimental models: Organisms/strains		
Macaque monkey (macaca mulatta)	N/A	N/A
Deposited data		
Raw data macaque L (Session L_RS_090817)	Chen et al. (2022)	https://doi.org/10.12751/g-node.i20kyh
Raw data macaque Y	This paper	Link will be provided upon publication
Software and algorithms		
Python 3	Python Software Foundation	https://python.org
Snakemake 7.32.4	Open Source	https://snakemake.readthedocs.io (Mölder et al., 2021)
Elephant 1.0.0	NeuralEnsemble	https://elephant.readthedocs.io (Denker et al., 2018)
Custom Code	Open Source	Link will be provided upon publication
Other		
Data acquisition system	Blackrock Microsystems LLC	https://blackrockneurotech.com/products/cerebus
Utah Array	Blackrock Microsystems LLC	https://blackrockneurotech.com/products/utah-array

Acknowledgements

We thank Julia Sprenger, Vahid Rostami and Emiliano Torre for previous work on artifacts. We thank Alexa Riehle for manually spike sorting the data of macaque Y. We thank Alexa Riehle and Thomas Brochier for providing the data of monkey Y. This project has received funding partly from the European Union's Horizon 2020 Framework Programme for Research and Innovation under Specific Grant Agreement No. 945539 (Human Brain Project SGA3), the NRW-network 'iBehave' (grant number: NW21-049) and by the Deutsche Forschungsgemeinschaft (DFG, German Research Foundation) - 368482240/GRK2416 and the DFG Priority Program (SPP 2041 "Computational Connectomics") [S.J.van Albada: AL 2041/1-1].

Author Contributions

Conceptualization, J.O., S.G. and J.I.; Methodology, J.O., A.M., S.E., A.K., S.G. and J.I.; Software, J.O., A.M., S.E., A.K. and J.I.; Formal Analysis and Investigation, J.O., A.M. and S.E. and J.I.; Visualization, J.O., A.M. and S.E.; Data Curation, A.M., S.E. and A.K.; Validation, S.E., S.G. and J.I.; Writing – Original Draft, J.O., A.M., S.E., A.K., S.G. and J.I.; Writing – Review & Editing, J.O., A.M., S.G. and J.I.; Funding Acquisition, S.G.; Resources, S.G.; Project Administration, J.O., S.G. and J.I.; Supervision, S.G. and J.I.

References

Barban, F., Chiappalone, M., Bonassi, G., Mantini, D., & Semprini, M. (2021). Yet another artefact rejection study: an exploration of cleaning methods for biological and neuromodulatory noise. Journal of Neural Engineering *18*, 0460c2.

Bell, A. J. & Sejnowski, T. J. (1995). An Information-Maximization Approach to Blind Separation and Blind Deconvolution. Neural Computation *7*, 1129–1159.

Blot, A. & Barbour, B. (2014). Ultra-rapid axon-axon ephaptic inhibition of cerebellar Purkinje cells by the pinceau. Nature Neuroscience *17*, 289–295.

Brochier, T., Zehl, L., Hao, Y., Duret, M., Sprenger, J., Denker, M., Grün, S., & Riehle, A. (2018). Massively parallel recordings in macaque motor cortex during an instructed delayed reach-to-grasp task. Scientific Data *5*, 180055.

Butts, D. A., Weng, C., Jin, J., Yeh, C.-I., Lesica, N. A., Alonso, J.-M., & Stanley, G. B. (2007). Temporal precision in the neural code and the timescales of natural vision. Nature *449*, 92–95.

Chen, X., Morales-Gregorio, A., Sprenger, J., Kleinjohann, A., Sridhar, S., van Albada, S. J., Grün, S., & Roelfsema, P. R. (2022). 1024-channel electrophysiological recordings in macaque V1 and V4 during resting state. Scientific Data *9*, 77.

Churchland, M. M., Yu, B. M., Ryu, S. I., Santhanam, G., & Shenoy, K. V. (2006). Neural variability in premotor cortex provides a signature of motor preparation. Journal of Neuroscience *26*, 3697–3712.

Dann, B., Michaels, J. A., Schaffelhofer, S., & Scherberger, H. (2016). Uniting functional network topology and oscillations in the fronto-parietal single unit network of behaving primates. eLife *5*, e15719.

de Haan, M. J., Brochier, T., Grün, S., Riehle, A., & Barthélemy, F. V. (2018). Real-time visuomotor behavior and electrophysiology recording setup for use with humans and monkeys. Journal of Neurophysiology *120*, 539–552.

Dehnen, G., Kehl, M. S., Darcher, A., Müller, T. T., Macke, J. H., Borger, V., Surges, R., & Mormann, F. (2021). Duplicate Detection of Spike Events: A Relevant Problem in Human Single-Unit Recordings. Brain Sciences *11*, 761.

Delorme, A., Sejnowski, T., & Makeig, S. (2007). Enhanced detection of artifacts in EEG data using higher-order statistics and independent component analysis. Neuroimage *34*, 1443–1449.

Denker, M., Yegenoglu, A., & Grün, S. (2018). Collaborative HPC-enabled workflows on the HBP Collaboratory using the Elephant framework. In Neuroinformatics 2018, p. P19.

Fabietti, M., Mahmud, M., Lotfi, A., Averna, A., Gugganmos, D., Nudo, R., & Chiappalone, M. (2020). Neural Network-based Artifact Detection in Local Field Potentials Recorded from Chronically Implanted Neural Probes. In 2020 International Joint Conference on Neural Networks (IJCNN), pp. 1–8. (Glasgow, United Kingdom: IEEE).

Farina, D., Merletti, R., Indino, B., & Graven-Nielsen, T. (2004). Surface EMG Crosstalk Evaluated from Experimental Recordings and Simulated Signals: Reflections on Crosstalk Interpretation, Quantification and Reduction. Methods of Information in Medicine *43*, 30–35.

Georgopoulos, A., Kalaska, J., Caminiti, R., & Massey, J. (1982). On the relations between the direction of two-dimensional arm movements and cell discharge in primate motor cortex. Journal of Neuroscience *11*, 1527–1537.

Grün, S. (2009). Data-driven significance estimation of precise spike correlation. Journal of Neurophysiology *101*, 1126–1140. (invited review).

Grün, S., Abeles, M., & Diesmann, M. (2008). Impact of higher-order correlations on coincidence distributions of massively parallel data. In Lecture Notes in Computer Science, 'Dynamic Brain - from Neural Spikes to Behaviors', vol. 5286.

Grün, S., Diesmann, M., & Aertsen, A. (2002a). Unitary events in multiple single-neuron spiking activity: I. detection and significance. Neural Computation *14*, 43–80.

Grün, S., Diesmann, M., & Aertsen, A. (2002b). Unitary events in multiple single-neuron spiking activity: II. nonstationary data. Neural Computation *14*, 81–119.

Grün, S., Diesmann, M., Grammont, F., Riehle, A., & Aertsen, A. (1999). Detecting unitary events without discretization of time. Journal of Neuroscience Methods *94*, 67–79.

Grün, S. & Rotter, S. eds. (2010). Analysis of Parallel Spike Trains. (Springer).

Harris, K. D., Quiroga, R. Q., Freeman, J., & Smith, S. L. (2016). Improving data quality in neuronal population recordings. Nature Neuroscience *19*, 1165–1174.

Hatsopoulos, N., Ojakangas, C., Paninski, L., & Donoghue, J. (1998). Information about movement direction obtained from synchronous activity of motor cortical neurons. Proceedings of the National Academy of Sciences of the United States of America *26*, 15706–15711.

Henze, D., Borhegyi, Z., Csicsvari, J.and Mamiya, A., Harris, K., & Buzsaki, G. (2000). Intracellular features predicted by extracellular recordings in the hippocampus in vivo. Journal of Neurophysiology *1*, 390–400.

Hotelling, H. (1936). Relations between two sets of variates. Biometrika *28*, 321–377.

Islam, M. K., Rastegarnia, A., Nguyen, A. T., & Yang, Z. (2014). Artifact characterization and removal for in vivo neural recording. Journal of Neuroscience Methods *226*, 110–123.

Jain, A., Kleinjohann, A., Graff, S., Doerenkamp, K., Kampa, B., Grün, S., & Musall, S. (2022). An adaptive analysis pipeline for automated denoising and evaluation of high-density electrophysiological recordings. 17 Mar 2022 - 20 Mar 2022, Lisbon(Portugal).

Jun, J. J., Steinmetz, N. A., Siegle, J. H., Denman, D. J., Bauza, M., Barbarits, B., Lee, A. K., Anastassiou, C. A., Andrei, A., Aydın, Ç., et al. (2017). Fully integrated silicon probes for high-density recording of neural activity. Nature *551*, 232–236.

Kilner, J. M., Baker, S. N., & Lemon, R. N. (2002). A novel algorithm to remove electrical cross-talk between surface EMG recordings and its application to the measurement of short-term synchronisation in humans. Journal of Physiology *538*, 919–930.

Koh, T. J. & Grabiner, M. D. (1993). Evaluation of methods to minimize cross talk in surface electromyography. Journal of Biomechanics *26*, 151–157.

König, P., Engel, A. K., Roelfsema, P. R., & Singer, W. (1995). How precise is neuronal synchronization. Neural Computation *7*, 469–485.

Ludwig, K. A., Miriani, R. M., Langhals, N. B., Joseph, M. D., Anderson, D. J., & Kipke, D. R. (2009). Using a Common Average Reference to Improve Cortical Neuron Recordings From Microelectrode Arrays. Journal of Neurophysiology *101*, 1679–1689.

Morales-Gregorio, A., Kurth, A. C., Ito, J., Kleinjohann, A., Barthélemy, F. V., Brochier, T., Grün, S., & van Albada, S. J. (2023). Neural manifolds in V1 change with top-down signals from V4 targeting the foveal region. BioRxiv pp. 2023–06.

Mumtaz, W., Rasheed, S., & Irfan, A. (2021). Review of challenges associated with the EEG artifact removal methods. Biomedical Signal Processing and Control *68*, 102741.

Musial, P., Baker, S., Gerstein, G., King, E., & Keating, J. (2002). Signal-to-noise ratio improvement in multiple electrode recording. Journal of Neuroscience Methods *1*, 29–43.

Mölder, F., Jablonski, K., Letcher, B., Hall, M., Tomkins-Tinch, C., Sochat, V., Forster, J., Lee, S., Twardziok, S., Kanitz, A., et al. (2021). Sustainable data analysis with snakemake [version 1; peer review: 1 approved, 1 approved with reservations]. F1000Research *10*.

Nagaoka, T., Walker, D., Seaba, P. J., & Yamada, T. (1992). "Cross-talk" in recording evoked potentials. Electroencephalography and Clinical Neurophysiology/Evoked Potentials Section *84*, 473–476.

Nelson, M. J., Valtcheva, S., & Venance, L. (2017). Magnitude and behavior of cross-talk effects in multichannel electrophysiology experiments. Journal of Neurophysiology *118*, 574–594.

Oberste-Frielinghaus, J. (2022). Baseline and Functional Correlations in Vision for Action Experiment. Master's thesis, RWTH Aachen University.

Pachitariu, M., Sridhar, S., & Stringer, C. (2023). Solving the spike sorting problem with kilosort. BioRxiv .

Perez-Prieto, N., Rodriguez-Vazquez, A., Alvarez-Dolado, M., & Delgado-Restituto, M. (2021). A 32-Channel Time-Multiplexed Artifact-Aware Neural Recording System. IEEE Transactions on Biomedical Circuits and Systems *15*, 960–977.

Pipa, G., Wheeler, D. W., Singer, W., & Nikolic, D. (2008). Neuroxidence: reliable and efficient analysis of an excess or deficiency of joint-spike events. Journal of Neuroscience Methods *25*, 64–88.

Pérez-Prieto, N. & Delgado-Restituto, M. (2021). Recording Strategies for High Channel Count, Densely Spaced Microelectrode Arrays. Frontiers in Neuroscience *15*, 681085.

Quiroga, R. Q. (2007). Spike sorting. Scholarpedia Journal *2*, 3583.

Quiroga, R. Q., Nadasdy, Z., & Ben-Shaul, Y. (2004). Unsupervised spike detection and sorting with wavelets and superparamagnetic clustering. Neural Computation *16*, 1661–87.

Rey, H. G., Pedreira, C., & Quian Quiroga, R. (2015). Past, present and future of spike sorting techniques. Brain Research Bulletin *119*, 106–117.

Riehle, A., Grün, S., Diesmann, M., & Aertsen, A. (1997). Spike synchronization and rate modulation differentially involved in motor cortical function. Science *278*, 1950–1953.

Riehle, A., Wirtssohn, S., Grün, S., & Brochier, T. (2013). Mapping the spatio-temporal structure of motor cortical LFP and spiking activities during reach-to-grasp movements. Frontiers in Neural Circuits *7*, 48.

Rong, F. & Contreras-Vidal, J. L. (2006). Magnetoencephalographic artifact identification and automatic removal based on independent component analysis and categorization approaches. Journal of Neuroscience Methods *157*, 337–354.

Semedo, J. D., Jasper, A. I., Zandvakili, A., Krishna, A., Aschner, A., Machens, C. K., Kohn, A., & Yu, B. M. (2022). Feedforward and feedback interactions between visual cortical areas use different population activity patterns. Nature Communications *13*, 1099.

Shackman, A. J., McMenamin, B. W., Slagter, H. A., Maxwell, J. S., Greischar, L. L., & Davidson, R. J. (2009). Electromyogenic Artifacts and Electroencephalographic Inferences. Brain Topography *22*, 7–12.

Snyder, A. C., Yu, B. M., & Smith, M. A. (2021). A Stable Population Code for Attention in Prefrontal Cortex Leads a Dynamic Attention Code in Visual Cortex. Journal of Neuroscience *41*, 9163–9176.

Steinmetz, N. A., Aydin, C., Lebedeva, A., Okun, M., Pachitariu, M., Bauza, M., Beau, M., Bhagat, J., Böhm, C., Broux, M., et al. (2021). Neuropixels 2.0: A miniaturized high-density probe for stable, long-term brain recordings. Science *372*, eabf4588.

Stella, A., Bouss, P., Palm, G., & Grün, S. (2022). Comparing surrogates to evaluate precisely timed higher-order spike correlations. eNeuro *9*, ENEURO.0505–21.2022.

Torre, E., Quaglio, P., Denker, M., Brochier, T., Riehle, A., & Grün, S. (2016). Synchronous spike patterns in macaque motor cortex during an instructed-delay reach-to-grasp task. Journal of Neuroscience *36*, 8329–8340.

Wim De Clercq, Vergult, A., Vanrumste, B., Van Paesschen, W., & Van Huffel, S. (2006). Canonical Correlation Analysis Applied to Remove Muscle Artifacts From the Electroencephalogram. IEEE Transactions on Biomedical Engineering *53*, 2583–2587.

Yu, B. M., Cunningham, J. P., Santhanam, G., Ryu, S. I., Shenoy, K. V., & Sahani, M. (2009). Gaussian-Process Factor Analysis for Low-Dimensional Single-Trial Analysis of Neural Population Activity. Journal of Neurophysiology *102*, 614–635.

Supplementary Material

Complexity distribution after removing all synchronous spikes

We examine the effect of the naive approach to remove all HSEs from the spike trains as proposed by Torre et al. (2016). Therefore we calculate the complexity distribution for the data after all spikes in HSEs are removed and compare this to the surrogates obtained from the data after the removal of the spikes. As to be expected, the distribution for the original data after the removal only contains entries for complexities of zero and one. However in the surrogates we find complexity up to six in the surrogate data, concluding that the data after removal significantly lacks synchrony since a certain amount of HSEs is expected. This shows that the naive approach should not be taken to remove synchrofacts.

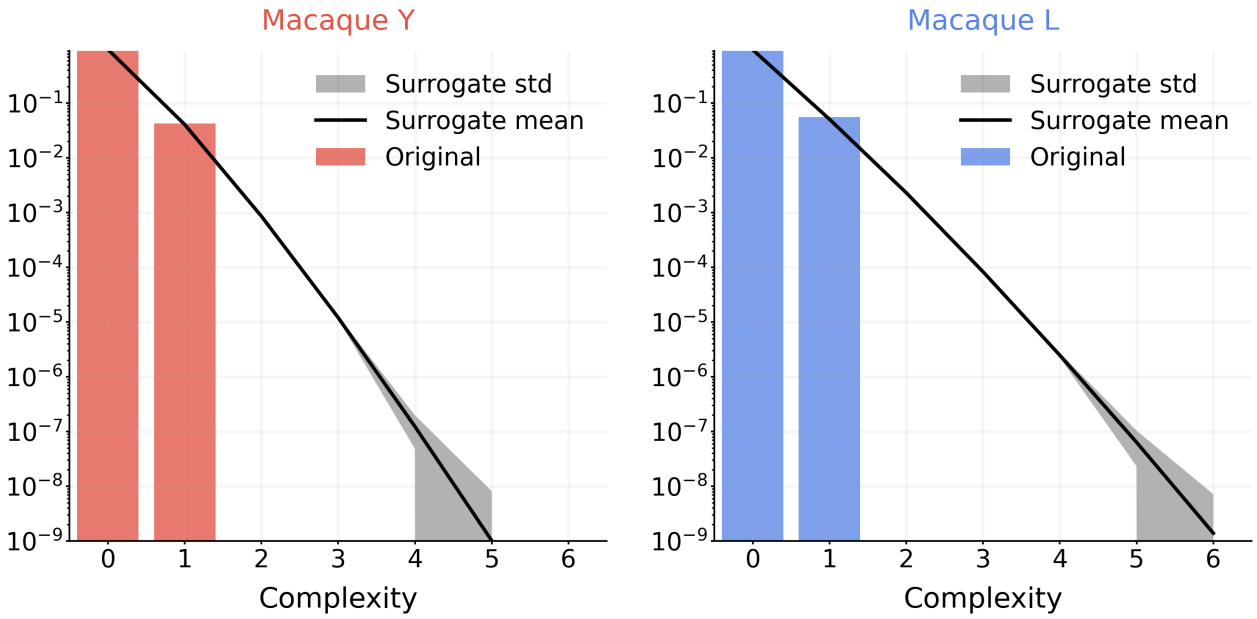

Figure S1: Complexity distribution after removing all synchronous spikes, Complexity distribution of the original data (colored bars), and the mean and standard deviation (line and shade, respectively) for the complexity distribution of the respective surrogates, $\frac{1}{30}$ ms bin size.

Connector mapping versus array mapping

In search for causes of strong raw signal correlations between channels, we examine the spatial distribution of the channels showing strong correlations on two spatial maps of channels: one on the level of the electrode arrays and the other the head stage connectors. In the case of macaque Y, the relative positions of channels are almost identical between the two maps, and hence we cannot conclude on which level the cross-talk is localized. In the case of macaque L, however, the spatial distribution of highly correlated channels is largely different between the array mapping and the connector mapping, indicating that the cause of the high correlations is localized on the level of the electrode arrays.

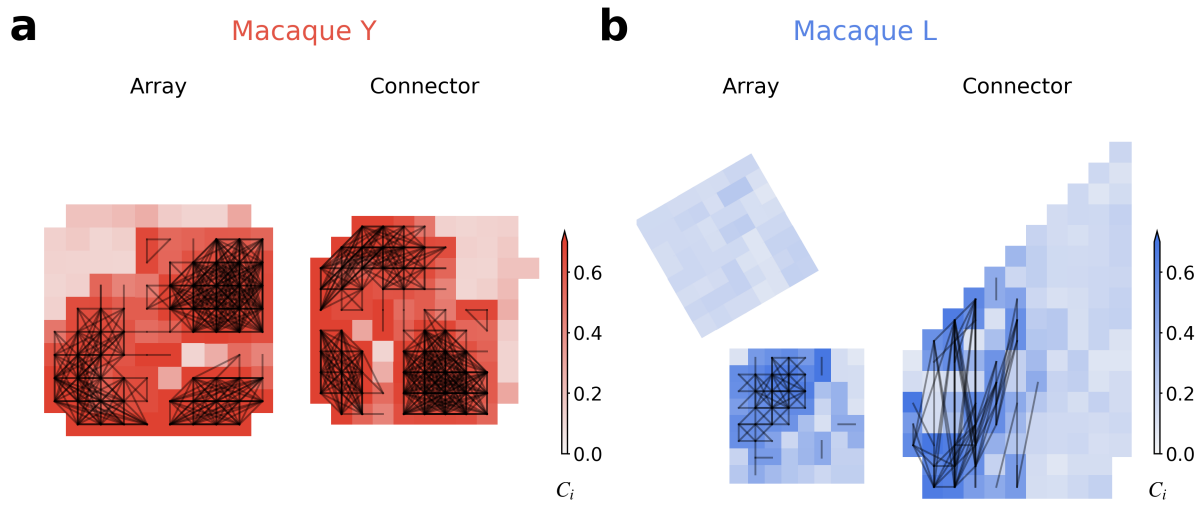

Figure S2: Comparison of spatial distribution of maximal raw signal correlation per channel (C_i) on the electrode array layout (left) and the headstage connector layout (right) for (a) macaque Y and (b) macaque L. Black lines connect electrode pairs with pairwise raw signal correlations $c_{i,j} > 0.4$.

Comparison between empirical and surrogate HSE index

To examine how large the HSE indices obtained from real data are in comparison to those from independent spike trains with matched firing rates, we plot the empirical pairwise HSE indices in the macaque Y data against the respective surrogate HSE indices obtained from time shifted surrogate data (Figure S3a; the mean over 200 surrogates is taken for each channel pair). The majority of channel pairs show larger empirical HSE index values than the respective surrogate values. This could reflect a bias originating from the definition of the HSE index that synchrofacts in channels with small numbers of spikes can be over-represented in the index. Hence, we next focus only on channels with firing rates greater than 1 spikes/s (Figure S3b). While a certain amount of channel pairs with large empirical HSE indices were screened out by this conditioning, we still see a considerable number of channels with extremely large empirical HSE indices compared to the surrogates, which are most likely the ones suffering from the cross-talk. After applying our proposed channel exclusion methods (Figure S3c and d), those channel pairs are screened out and the remaining ones show empirical HSE indices comparable to the surrogate indices, meaning that the remaining channels have as many HSEs as in independent spike trains. The mean of the empirical HSE indices over channel pairs is still slightly higher than the mean of the surrogate HSE indices, which is likely due to other causes of synchrofact than cross-talk. One of such causes is common external noise across channels. Spike-like events generated by such noise typically show waveforms dissimilar to real spike waveforms, and hence can be effectively excluded by spike sorting. To check whether that is actually the case, we plot the HSE indices for SUA pairs in the same manner as before (Figure S3e-g). Again, after applying our proposed methods, SUA pairs show only as many HSEs as in the surrogates, and in this case of SUA pairs, the mean empirical HSE index is much more consistent with the mean surrogate HSE index than in the case of channel pairs.

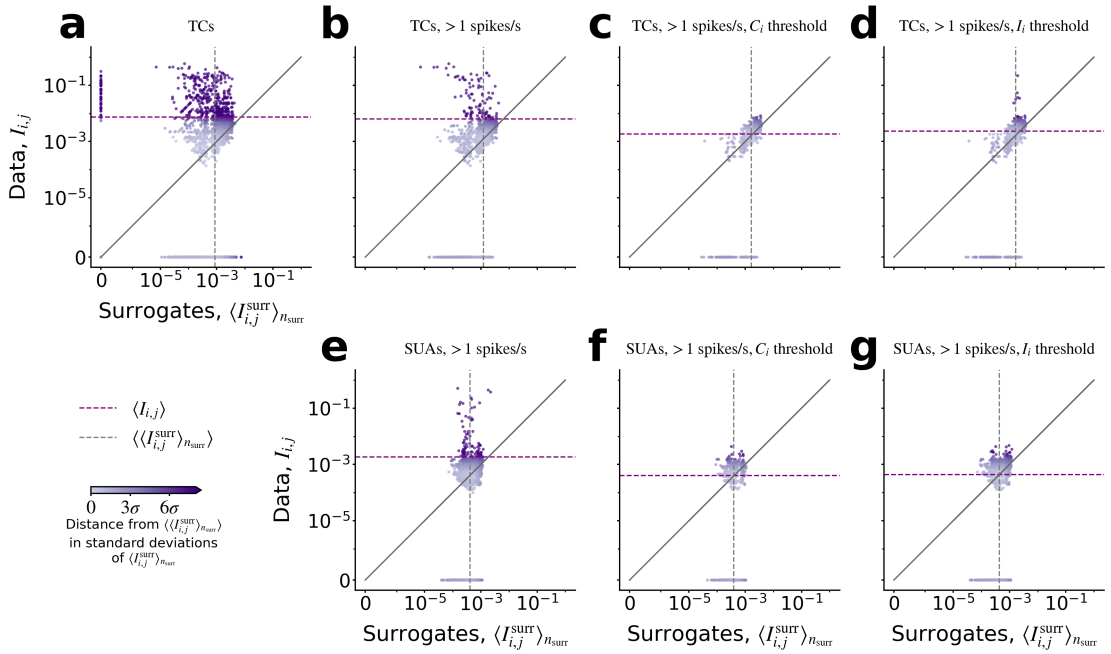

Figure S3: Comparison of the pairwise HSE index $I_{i,j}$ in the experimental data and the average of the corresponding surrogate data $\langle I_{i,j}^{\mathrm{surr}} \rangle_{n_{\mathrm{surr}}}$, each point corresponding to one channel pair. Mean of each variable is shown with a dashed line. The diagonal line indicates the identity between the two measures. The color shading represents the difference from the theoretically random data, at the point where the mean surrogate index $\langle \langle I_{i,j}^{\mathrm{surr}} \rangle_{n_{\mathrm{surr}}} \rangle$ crosses the diagonal; large deviations from this point are indicative of above-chance HSEs. The different panels show the results for the same session based on (a-d) all threshold crossings (TCs), or (e-g) spike sorted single units (SUAs). The different columns show different removal methods: (b, e) threshold on the firing rate, (c, f) threshold on firing rate and maximum cross-correlation C_i, and (d, g) threshold on firing rate and global HSE index I_i.

Common noise artifact example

The data of macaque L contained highly synchronized activity in the data lasting for about 500 ms (see Figure S4, bottom), which is likely due to strong common noise contaminating all the channels equally. Such common noise can enter the system via the reference electrode. We identified this burst of synchronous spike activity as artifacts since these synchronous spikes also still exist on the sampling rate resolution (top). It introduced in the complexity distribution a huge amount of events with complexities up to 35. Therefore, we removed this piece of data (1000 ms) before any further analysis. We did not detect such events in the data from macaque Y.

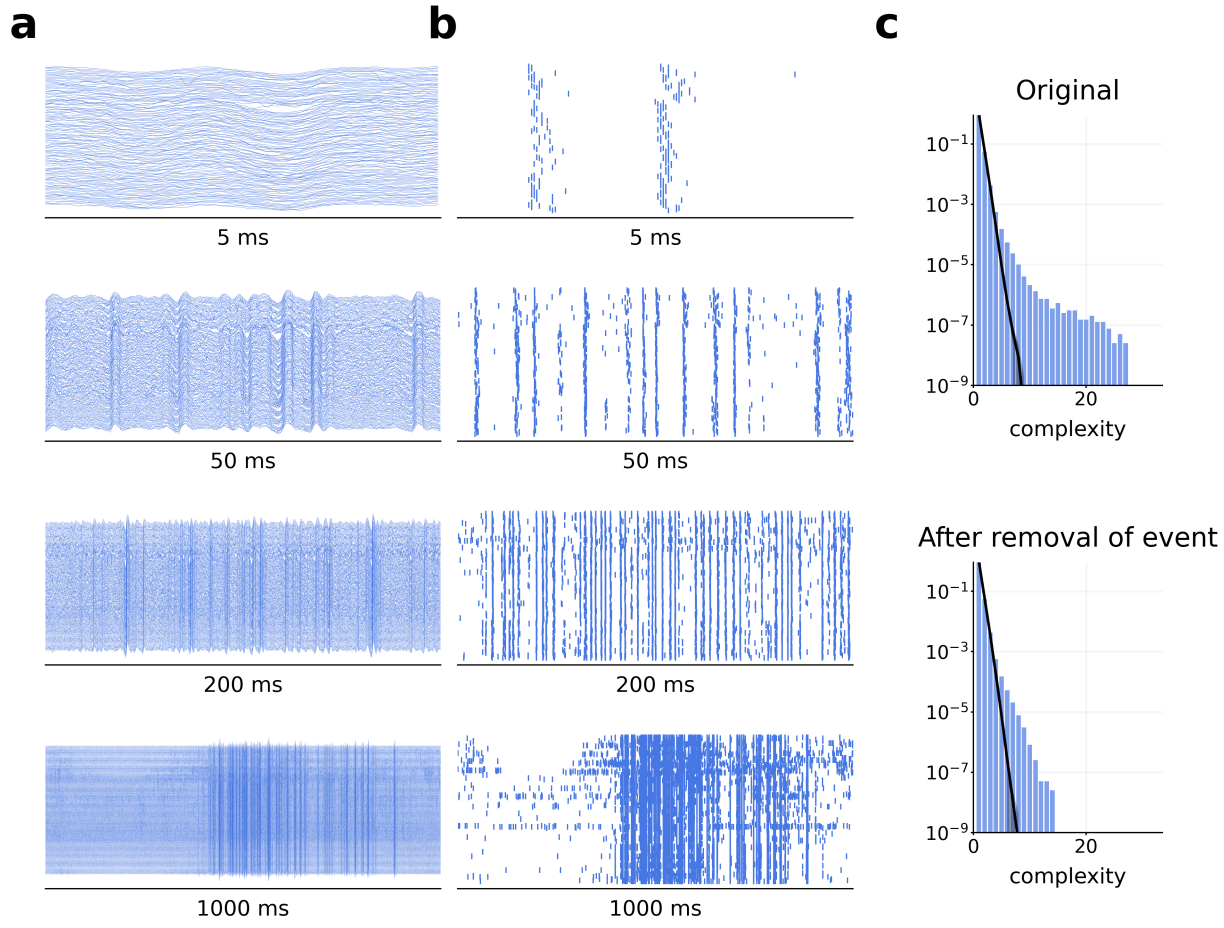

Figure S4: Burst artifact in monkey L. The left column, bottom shows the whole burst artifact, that expresses a lot of synchrofacts (on sampling rate of 30 kHz) one after the other over a period of about 500 ms. The plots above show higher resolutions of that event, and on the top the total display shows piece of the data lasting 5 ms. On the right top, the complexity distribution of the whole data set is shown, below after the complete removal of this burst event, which still contains artifacts. But as shown in Figure 5 these can be completely removed by our removal procedure.